

Chapter 5

Location of the innermost stable circular orbit of binary neutron stars in the post Newtonian approximations of general relativity

Masaru Shibata, Keisuke Taniguchi* and Takashi Nakamura†

*Department of Earth and Space Science, Graduate School of Science,
Osaka University, Toyonaka, Osaka 560, Japan*

** Department of Physics, Kyoto University, Kyoto 606-01, Japan*

† Yukawa Institute for Theoretical Physics, Kyoto University, Kyoto 606-01, Japan

Abstract

In this paper, we present results obtained from our recent studies on the location of the innermost stable circular orbit (ISCO) for binary neutron stars (BNSs) in several levels of post Newtonian (PN) approximations. We reach the following conclusion at present: (1) even in the Newtonian case, there exists the ISCO for binary of sufficiently stiff equation of state (EOS). If the mass and the radius of each star are fixed, the angular velocity at the ISCO Ω_{ISCO} is larger for softer EOS: (2) when we include the first PN correction, there appear roughly two kinds of effects. One is the effect to the self-gravity of each star of binary and the other is to the gravity acting between two stars. Due to the former one, each star of binary becomes compact and the tidal effect is less effective. As a result, Ω_{ISCO} tends to be increased. On the other hand, the latter one has the property to destabilize the binary orbit, and Ω_{ISCO} tends to be decreased. If we take into account both effects, however, the former effect is stronger than the latter one, and Ω_{ISCO} becomes large with increase of the 1PN correction: (3) the feature mentioned above is more remarkable for softer EOS if the mass and radius are fixed. This is because for softer EOS, each star has the larger central density and is susceptible to the GR correction: (4) there has been no self consistent calculation including all the 2PN effects and only exist studies in which one merely includes the effect of the 2PN gravity acting between two stars. In this case, the effect has the property to destabilize the binary orbit, so that Ω_{ISCO} is always smaller than that for the Newtonian case. If we include the PN effect of the self-gravity to each star, Ω_{ISCO} will increase.

§1. Introduction

BNSs like PSR1913+16 are believed to be formed after the second supernova explosion in the evolution of massive binary stars. At the formation, orbits of BNSs will be highly eccentric because a large amount of the mass of the system is ejected in the supernova explosion. If the semi-minor axis of BNSs is less than about a few times of solar radius, they will coalesce within the age of the universe $\sim 10^{10}$ yr due to the emission of gravitational waves (GWs). In the evolution of the binary the orbital radius as well as the orbital eccentricity decreases so that the orbit becomes almost circular when the orbital radius is about 10^2 times of the neutron star (NS) radius where the frequency of GWs is ~ 10 Hz, i.e., in the frequency band sensitive

to the kilometer size laser interferometric GW detector such as LIGO,¹⁾ VIRGO,²⁾ GEO600,³⁾ and TAMA.⁴⁾ After that, evolution of BNSs is divided into two phases: One is the so called inspiraling phase where the orbital radius of BNSs is sufficiently larger than the radius of each NS. In this phase, the hydrodynamic effect of NS is not so important for the orbital evolution that each star of binary is approximately regarded as a point mass. The emission time scale of gravitational waves (GWs), t_{GW} , is still much longer than the orbital period and as a result, the circular orbit of BNSs is stable, so that BNSs evolve adiabatically in the inspiraling phase. The second phase is the post inspiraling phase in which the orbital radius becomes a few times of the NS radius and the hydrodynamic effect as well as general relativistic (GR) effects between two stars become very important. Just after BNSs enter this phase, i.e., the orbital radius of BNSs becomes smaller than the innermost stable circular orbit (ISCO), the circular orbit becomes unstable due to the hydrodynamic and GR effects and BNSs come into a final plunging and merging phase.

GWs in the inspiraling phase have a characteristic feature; the Fourier spectrum of the signal behaves as $\propto f^{-7/6}$.⁵⁾ However, when the BNSs enter the post inspiraling phase, their wave form will change drastically because the motion of the BNSs changes from circular orbit to plunging one. In particular, the ISCO is the characteristic orbit of such transition. The transition point will be sensitively determined by mass-radius relation of NS^{6) 7)} and the EOS of NSs may be determined from the mass-radius relation.⁸⁾ Hence, the signal around the ISCO will have important information on the equation of state (EOS), or in other words, the internal structure of NS. This means that if we detect a signal from BNSs at the ISCO, we will be able to constrain the EOS by comparing the signal with theoretical templates. For this reason, theoretical studies for the ISCO are urgent.

In Fig.1, we schematically show the location of the ISCO in each level of approximation which has been determined from recent studies: In the Newtonian case, there does not exist the ISCO if we regard each star of binary as point masses, but it appears for BNSs of sufficiently stiff EOS if we take into account the hydrodynamic effect on BNSs.^{9) 10)} This is because each star is tidally deformed by the gravity from the companion star and the tidal deformation induces the attractive force which overcomes the centrifugal force at small radius. For soft EOS, the degree of the central condensation is high, so that the effect of tidal force is not so important compared with the stiff EOS case.

When we include the first PN (1PN) correction of general relativity, not only the gravity between two stars, but also the self-gravity in each star become stronger than those in the Newtonian case. If the former effect is stronger than the latter one, the orbital radius of the ISCO (R_{ISCO}) becomes larger than that in the Newtonian case, because the former PN effect has the property to destabilize circular orbits as we will show later (§3 and §4). On the other hand, if the opposite relation holds, R_{ISCO} becomes smaller than that in the Newtonian case because each star of binary is forced to be compact due to the PN correction of the self-gravity and the tidal effect is less important. Recently, investigating equilibrium sequences of corotating binary, Shibata and Taniguchi found that the latter effect is stronger than the former one^{11) 12) 13)}, and R_{ISCO} becomes small due to the 1PN correction. As a result, the

angular frequency at the ISCO increases.

Another approach has been performed by Taniguchi and Nakamura (TN)¹⁴⁾ as well as Lai and Wiseman (LW)¹⁵⁾ and Ogawaguchi and Kojima.¹⁶⁾ Note that the methods adopted by three groups are essentially similar. In their approaches, they include the second PN (2PN) corrections and some parts of the higher relativistic corrections to the gravity between two stars phenomenologically, although they do not take into account the PN terms to the self-gravity of each star using the Newtonian equilibrium. In this case, the PN attractive force between two stars tends to destabilize circular orbits and as a result, R_{ISCO} becomes larger while the angular velocity becomes smaller compared with the point particle cases.

Considering these recent developments for understanding the mechanism which determines the ISCO, we organize this paper as follows. We analyze equilibrium sequences of binary stars assuming that t_{GW} is sufficiently larger than the orbital period, and argue the stability of binary along the sequence because the ISCO is just the critical point of stability. In §2, after we briefly mention why the ISCO exists even in the Newtonian case, we describe how the location of the ISCO for fluid stars is determined paying particular attention to the incompressible star. In the latter part of §2, we also argue the effect of the EOS analyzing equilibrium states of corotating binary of compressible stars. In §3 and §4, analyzing equilibrium states of corotating binaries, we argue how the location of the ISCO changes due to the 1PN correction for incompressible and compressible fluid cases, respectively. In the incompressible case, it is possible to obtain a fairly accurate analytic solution of corotating binaries even in the 1PN case, so that in §3, we present the method to derive it in detail. On the other hand, in the compressible case, we cannot obtain the analytic solution, so that we perform numerical computations and show the results in §4. In §5, we review the method and results by TN in which the 2PN and some parts of the higher PN corrections are taken into account only for the gravity acting between two stars. As mentioned above, the results they (and LW) obtained seem to apparently disagree with those by the full 1PN study. One of the reasons for this difference is the starting point of the problem. In the 1PN case, the zeroth order solution is the Newtonian equilibrium and then 1PN effect is taken into account as the correction. While in treatment of TN, a semi-relativistic equation of motion (EOM) for point particle with ISCO is the zeroth order equation and then the finite size effect of the star is taken into account. Another reason is the consistency of the treatment. In the 1PN case, 1PN effects of the gravity are consistently taken into account to both the self-gravity of each star and the gravity between two stars. While in TN, only 2PN and the some part of the higher order effects of gravity between two stars are considered phenomenologically. To understand the effect of the self-gravity more clearly, in the last subsection of §5, we compute 1PN ISCO removing the 1PN self-gravity force in §3. From the results, we suggest that if we include the 1PN effect of the self-gravity in TN, R_{ISCO} will decrease. We briefly review recent semi-GR calculations in §6. Section 7 is devoted to summary.

Throughout this paper, we use G and c as the gravitational constant and the speed of light. We define the Newtonian mass M and the multipole moment $I_{ijk\dots}$

as

$$M = \int \rho d^3x \quad \text{and} \quad I_{ijk\dots} = \int \rho x_i x_j x_k \dots d^3x, \quad (1.1)$$

where ρ denotes the baryon density of star and the integral is performed inside each star of binary. We also define the tracefree part of the quadrupole moment as

$$\mathcal{I}_{ij} = I_{ij} - \frac{1}{3} \delta_{ij} \sum_{k=1}^3 I_{kk}, \quad (1.2)$$

where δ_{ij} denotes the Kroneker's δ .

In the following sections, we take the axis for the orbital motion of binary as x_3 , and two stars have equal Newtonian mass M and the same structure for simplicity. In §2.1, §3 and §5, we put the center of the star 1^{*)} at the origin and center of the star 2 at $(-R, 0, 0)$ (i.e., the orbital separation is R and x_1 axis is the semimajor axis; see Fig.2), and consider the hydrostatic equilibrium for star 1. Orbital rotation is assumed to be counterclockwise in all sections.

§2. ISCO for binary neutron stars in the Newtonian theory

For binary of two point particles in the Newtonian theory, it is well known that there is no ISCO: In this case, the energy conservation equation can be written as¹⁷⁾

$$\frac{m}{2} \left(\frac{dr}{dt} \right)^2 = E - V(r); \quad V(r) = \frac{m\ell^2}{2r^2} - \frac{GM_t m}{r}, \quad (2.1)$$

where m , M_t , ℓ , E , r and t denote the reduced mass, total mass of the binary, the specific angular momentum, the energy, the orbital separation, and the coordinate time, respectively. The circular orbit of its radius $r_0 = \ell^2/GM_t$ is always stable up to the contact of binary because d^2V/dr^2 is always positive at $r = r_0$.

We can also explain the stability of the circular orbit in the following way: The energy of the circular orbit is

$$E = -\frac{GM_t m}{2r_0}. \quad (2.2)$$

This expression means that if $E < 0$, the circular orbit always exists up to $r_0 = 0$. This also shows the existence of the stable circular orbit for $0 < r_0 < \infty$. Note that this conclusion follows from the fact that the centrifugal force is always stronger than the gravitational force at small radii ($r < r_0$).

This is not necessarily the case for NS case if we remind the finite extension of the star and take into account the hydrodynamic effect on each NS. Due to the tidal field from the companion star, each NS of BNSs will be tidally deformed. In such a case, $V(r)$ is approximately written as

$$V(r) = \frac{m\ell^2}{2r^2} - \frac{GM_t m}{r} - \frac{3GM_t}{2r^3} \mathcal{I}_{11}(t), \quad (2.3)$$

^{*)} Here, “the center of mass” indicates that defined in the Newtonian order. We should be careful to define it in the PN order (see §3).

where we assume that the center of each star is located on the x_1 axis and \mathcal{I}_{11} is 11 component of the tracefree part of the quadrupole moment of each star. Here, we only take into account the lowest order multipole among all the multipole moments which are generated by the tidal deformation. We note that \mathcal{I}_{11} changes approximately as $O(r^{-3})$ if the star does not have an intrinsic spin. So that the third term in Eq. (2.3) behaves as $O(r^{-6})$ in reality. Thus, the effect of the tidal deformation is very small for large r , but it cannot be negligible in the case of small r . If the tidal deformation is sufficiently large, it may overcome the centrifugal potential for a sufficiently small r , and in such a case, the orbit becomes unstable before each star of binary comes into contact; i.e., for $E < E_{\text{crit}}$ where E_{crit} is a critical value of the energy, no circular orbit exists. This is essentially what Lai, Rasio, and Shapiro (LRS) pointed out^{9) 10)} already.

2.1. Incompressible case

We explain the qualitative fact mentioned above by showing sequences of equilibrium states of incompressible binary stars in more details. In the Newtonian case, the hydrostatic equation in the rotating frame of the angular velocity Ω is¹⁸⁾

$$\rho \sum_{j=1}^3 u_j \frac{\partial u_i}{\partial x_j} = -\frac{\partial P}{\partial x_i} + \rho \frac{\partial}{\partial x_i} \left[U + \frac{\Omega^2}{2} \left\{ \left(x_1 + \frac{R}{2} \right)^2 + x_2^2 \right\} \right] + 2\rho\Omega \sum_{l=1}^3 \epsilon_{il3} u_l, \quad (2.4)$$

where u_i , P , and ϵ_{ijk} denote the velocity in the rotating frame, the pressure, and the completely antisymmetric tensor, respectively. U is the Newtonian potential which satisfies

$$\Delta U = -4\pi G\rho, \quad (2.5)$$

and it can be split into two parts; one is the self-gravity part, and the other is the contribution from the companion star. We separate U as

$$U = U^{1 \rightarrow 1} + U^{2 \rightarrow 1}, \quad (2.6)$$

where $U^{1 \rightarrow 1}$ denotes the self-gravity part and $U^{2 \rightarrow 1}$ denotes the contribution from the companion. These are written, respectively, as

$$U^{1 \rightarrow 1} = \pi G\rho \left(A_0 - \sum_{i=1}^3 A_i x_i^2 \right), \quad (2.7)$$

$$U^{2 \rightarrow 1} = \frac{GM}{R} \left(1 - \frac{x_1}{R} + \frac{2x_1^2 - x_2^2 - x_3^2}{2R^2} + \frac{-2x_1^3 + 3x_1(x_2^2 + x_3^2)}{2R^3} + O(R^{-4}) \right) + \frac{3G\mathcal{I}_{11}}{2R^3} \left(1 - \frac{3x_1}{R} + O(R^{-2}) \right), \quad (2.8)$$

where we only include the contribution from the quadrupole moment of each star, and neglect the higher multipoles. In this case, we may assume that each star of binary is an ellipsoid of its axial length a_1 , a_2 and a_3 . Index symbol A_i is that defined in the textbook of Chandrasekhar¹⁸⁾ and $A_0 = \sum_i A_i a_i^2$ is calculated from

$$A_0 = a_1^2 \alpha_2 \alpha_3 \int_0^\infty \frac{dt}{\sqrt{(1+t)(\alpha_2^2+t)(\alpha_3^2+t)}} \equiv a_1^2 \tilde{A}_0(\alpha_2, \alpha_3), \quad (2.9)$$

where $\alpha_2 = a_2/a_1$ and $\alpha_3 = a_3/a_1$. Note that A_i is the function of α_2 and α_3 ¹⁸).

For ellipsoids, the pressure P is given by

$$P = P_0 \left(1 - \sum_{i=1}^3 \frac{x_i^2}{a_i^2} \right). \quad (2.10)$$

Hereafter, we assume for simplicity that the internal motion of one star is the same as that of the other star, and we restrict its form given as

$$u_1 = \frac{a_1}{a_2} \Lambda x_2 \quad u_2 = -\frac{a_2}{a_1} \Lambda x_1. \quad (2.11)$$

In this case, the vorticity $\omega = 2\Omega + \sum_{j,k} \epsilon_{3jk} \partial_j u_k$ in the inertial frame is spatially constant everywhere inside the star as

$$\omega = 2\Omega - \left(\frac{a_2}{a_1} + \frac{a_1}{a_2} \right) \Lambda \equiv \Omega(2 + f_R); \quad f_R \equiv -\frac{a_1^2 + a_2^2}{a_1 a_2} \frac{\Lambda}{\Omega}. \quad (2.12)$$

Thus, the circulation in the equatorial plane becomes

$$C = \pi a_1 a_2 \Omega (2 + f_R). \quad (2.13)$$

From the first tensor virial (TV) relation, we obtain the orbital angular velocity as

$$\Omega^2 = \frac{2GM}{R^3} + \frac{18G\mathcal{I}_{11}}{R^5}. \quad (2.14)$$

From the second TV relation, we obtain the following three equations;

$$\begin{aligned} -\Lambda^2 &= \frac{2P_0}{\rho a_1^2} - 2\pi G\rho A_1 + \frac{2GM}{R^3} + \Omega^2 - 2\frac{a_2}{a_1} \Lambda \Omega, \\ -\Lambda^2 &= \frac{2P_0}{\rho a_2^2} - 2\pi G\rho A_2 - \frac{GM}{R^3} + \Omega^2 - 2\frac{a_1}{a_2} \Lambda \Omega, \\ 0 &= \frac{2P_0}{\rho a_3^2} - 2\pi G\rho A_3 - \frac{GM}{R^3}. \end{aligned} \quad (2.15)$$

Note that relations among R/a_1 , α_2 and α_3 are derived from these three equations.

The energy and the angular momentum are calculated as

$$\begin{aligned} E &= \frac{M}{5} \left[\left(\Omega - \frac{a_2}{a_1} \Lambda \right)^2 a_1^2 + \left(\Omega - \frac{a_1}{a_2} \Lambda \right)^2 a_2^2 \right] + \frac{MR^2}{4} \Omega^2 \\ &\quad - \frac{4}{5} \pi G\rho M A_0 - \frac{GM}{R} \left(M + \frac{3\mathcal{I}_{11}}{R^2} \right), \end{aligned} \quad (2.16)$$

$$J = \frac{2M}{5} (a_1^2 + a_2^2) \Omega - \frac{4M}{5} a_1 a_2 \Lambda + \frac{MR^2}{2} \Omega. \quad (2.17)$$

In Eq. (2.16), the terms in brackets $[\dots]$ denote the spin kinetic energy of each star, the next two terms denote the kinetic energy of the orbital motion and the binding

energy by the self-gravity, and the final two terms denote the binding energy between two stars. The sum of the kinetic energy of the orbital motion and the binding energy between two stars mainly concerns the stability of the orbit and it becomes

$$-\frac{GM^2}{2R} + \frac{3M\mathcal{I}_{11}}{2R^3}. \quad (2.18)$$

Since $a_1 > a_2, a_3$ and as a result $\mathcal{I}_{11} > 0$, the second term is positive definite. Thus, the energy has a minimum critical value E_{crit} at a small radius due to the second term. As mentioned above, this just indicates that the tidal effect acts as the destabilization.

Before presenting results on equilibrium states, we mention the possible state of internal motion of star. If the viscosity of the fluid is so small that the dissipation time scale of the circulation by the viscosity (t_{vis}) is much longer than t_{gw} , the circulation conserves throughout the whole evolution. On the other hand, if the viscosity is so large that t_{vis} is shorter than t_{gw} , BNSs will settle down to the corotating configuration. Kochanek, and Bildsten and Cutler showed that in order to achieve corotating binary dissipating the circulation, the viscosity must satisfy¹⁹⁾

$$\eta \gtrsim 10^{29} \left(\frac{R}{a_0}\right)^2 \left(\frac{M}{1.4M_\odot}\right)^4 \left(\frac{10\text{km}}{a_0}\right)^5 \text{ g/cm/s}, \quad (2.19)$$

where $a_0 = (3M/4\pi\rho)^{1/3}$ and M_\odot denotes the solar mass. Since this value is much larger than the microscopic viscosity,²⁰⁾ we should consider sequences of equilibrium states of constant C as realistic BNSs.

By the way, for large $R \rightarrow \infty$, $\Omega \rightarrow 0$, so that $C \rightarrow -\pi(a_1^2 + a_2^2)A$. This implies that $-A$ at $R \rightarrow \infty$ is regarded as the intrinsic spin angular velocity of each star (we denote it as Ω_s following LRS¹⁰⁾). Since $|\Omega_s|$ for real NS's will be less than $\sim 0.6\Omega_0$, where $\Omega_0 \equiv (GM/a_0^3)^{1/2}$,^{21) 22)} $|C|$ should be less than $\sim 4(GMa_0)^{1/2}$. Note that for pulsars we have ever known,²³⁾ $|\Omega_s| \lesssim 0.2\Omega_0$.

In Figs.3, we show the energy and angular momentum as functions of Ω/Ω_0 for $C/(GMa_0)^{1/2} = -2 \sim 2$. We also show them for corotating binary for comparison. We see that there exists a critical angular velocity where the energy and angular momentum are simultaneously minima. As LRS showed,⁹⁾ the minima in the energy and angular momentum along the constant- C sequence indicate the onset of dynamical instability. Thus, the minimum corresponds to the ISCO. As mentioned above, this minimum occurs due to the tidal interaction between two stars at small separation. Each star deforms and the quadrupole dependent term in the effective interaction potential between two stars (i.e., the third term in Eq. (2.3)) becomes sufficiently large.

Figures 3 also show some important features for the ISCO. First, the effect of the spin of each star is not so important in determining the ISCO as long as it is not very large, i.e., $|C|/(GMa_0)^{1/2} < 1$. Second, even for corotating sequence where the circulation does not conserve, there exists a critical angular velocity where the energy and angular momentum are simultaneously minima, and it locates near the minima for constant- C sequence. Although the minima for corotating sequence do

not mean the onset of the dynamical instability, but of the secular instability⁹⁾ (so we call it the innermost stable corotating circular orbit (ISCCO)), its existence is useful for analysis of the ISCO. This is because the angular velocity at the minima for corotating sequence is only slightly smaller than that for constant- C (small C) sequences and as a result, we can approximately find the location of the ISCO for constant- C sequences by investigating corotating sequence instead.

2.2. Compressible case

Next, we argue the effect of EOS. Since the location of the ISCO for binary stars is determined by the degree of the tidal deformation, it depends on the EOS of NS. NS becomes more centrally concentrated as the EOS is softer. Thus, the tidal effect is less important for softer EOS. This means that the effect of EOS is quantitatively very important in determining the location of the ISCO. Actually, using an approximate analytical model, LRS have shown that if we assume the polytropic EOS as

$$P = K\rho^\Gamma; \quad \Gamma = 1 + \frac{1}{n}, \quad (2.20)$$

where K and n are the polytropic constant and the polytropic index, R_{ISCO} is smaller for larger n , and for sufficiently large n ($\gtrsim 1$), the ISCO disappears.

Although LRS presented approximate locations of the ISCO for various n , we do not know the precise ones. Furthermore, their approximation is good only for small n , so that quantitative dependence on the EOS may not be understood well for realistic NS whose EOS has $0.5 \lesssim n \lesssim 1$.²²⁾ To get precise locations of the ISCO, we need to perform numerical calculation, but we have not yet established an accurate numerical method of obtaining equilibrium states including arbitrary circulation. As we mentioned above, however, corotating sequence may be regarded as an approximate sequence of constant circulation if the spin of each star is not so large, and we have accurate methods of obtaining corotating sequences.²⁴⁾ Thus, we here see the effect of the EOS by investigating corotating sequences.

Equilibrium states of corotating binary stars are obtained by consistently solving the Newtonian potential U and the integrated Euler equation as

$$K(n+1)\rho^{1/n} = U + \frac{\varpi^2}{2}\Omega^2; \quad \varpi^2 = \left(x_1 + \frac{R}{2}\right)^2 + x_2^2. \quad (2.21)$$

In Figs.4, we show the energy and the angular momentum as functions of the angular velocity for $n = 0.25, 0.5, 0.75$ and 1 ($\Gamma = 5, 3, 7/3$ and 2). The energy, angular momentum, and angular velocity are shown in units of GM^2/a_0 , $(GM^3a_0)^{1/2}$, and $\Omega_0 \equiv (GM/a_0^3)^{1/2}$, respectively, where a_0 denotes the radius of the spherical polytropic star. In each figure, the circle of the largest Ω denotes the configuration at contact of two stars. It is found from figs.4 that with increase of n , Ω at the energy and angular momentum minima increases and the minima tend to disappear for given a_0 and M . The angular velocity at the minima, $\Omega_{\text{N:ISCCO}}$, is $\simeq (0.252 - 0.256)\Omega_0$ for $n = 0.25$, $\simeq (0.265 - 0.269)\Omega_0$ for $n = 0.5$, $\simeq (0.279 - 0.283)\Omega_0$ for $n = 0.75$ and $\simeq (0.296 - 0.298)\Omega_0$ for $n = 1$.^{*)} Note that for incompressible case, it is $\simeq 0.248\Omega_0$.

^{*)} Note that in the analysis by LRS,⁹⁾ they somewhat overestimate $\Omega_{\text{N:ISCCO}}$ for compressible

From these numerical results, the angular velocity at the minima for compressible star of $n = 0 - 1$ is found to be approximately expressed as (see Fig.5)

$$\Omega_{\text{N:ISCCO}} \simeq 0.248(1 + 0.2n^\alpha)\Omega_0, \quad (2.22)$$

where $\alpha \sim 1.5$. Thus, the frequency of GWs corresponding to $\Omega_{\text{N:ISCCO}}$ is calculated from $f_{\text{N:ISCCO}} \equiv \Omega_{\text{N:ISCCO}}/\pi$, which is

$$f_{\text{N:ISCCO}} \simeq 590(1 + 0.2n^{1.5}) \left(\frac{M}{1.4M_\odot} \right)^{1/2} \left(\frac{15\text{km}}{a_0} \right)^{3/2} \text{ Hz}. \quad (2.23)$$

The above results concerning the dependence of the energy and angular momentum minima on the EOS are for corotating binaries, but we may expect that similar dependence holds for constant- C sequences if the spin of each star is not so large. This is because change of the EOS mainly affects the density profile of each star almost independent of the spin and circulation. Actually, from the results by an approximate study of LRS,⁹⁾ it is found that the following quantity is almost independent of the EOS;

$$\frac{\Omega_{\text{N:ISCO}} \text{ for } C = 0 \text{ sequence}}{\Omega_{\text{N:ISCCO}} \text{ for corotating sequence}}. \quad (2.24)$$

Thus, we are allowed to conclude that even for constant- C sequences the angular frequency at the ISCO for compressible star will increase approximately with $n^{1.5}$ as Eq. (2.22).

§3. First post Newtonian study: Incompressible case

In §2, we briefly mention that the ISCO exists even in the Newtonian case if the EOS of NS is sufficiently stiff. In this section, we see how the location of the ISCO obtained in the Newtonian theory is affected by the 1PN correction of general relativity. We again make use of sequences of corotating binary stars. In this section, as a first step, we investigate equilibrium states for incompressible binary stars for which fairly accurate approximate solutions are obtained in an analytic manner (see details in Ref. 12)).

3.1. Formulation

Non-axisymmetric equilibrium configurations of uniformly rotating incompressible fluid in the 1PN approximation are obtained by solving the integrated form of the Euler equation and the Poisson equations for gravitational potentials consistently. The integrated form of the Euler equation was derived by Chandrasekhar²⁵⁾ and it can be written as^{11) 26)*)}

$$\int \frac{dP}{\rho} - \frac{1}{c^2} \int \left(\varepsilon + \frac{P}{\rho} \right) \frac{dP}{\rho}$$

star. For example, $\Omega_{\text{N:ISCCO}} = 0.279\Omega_0$ for $n = 0.5$ and $\Omega_{\text{N:ISCCO}} = 0.314\Omega_0$ for $n = 1$ in their analysis.

*) Note that we use the standard PN gauge.

$$= U - \frac{X_0}{c^2} + \left\{ \frac{\varpi^2}{2} + \frac{1}{c^2} (2\varpi^2 U - X_\Omega + \hat{\beta}_\varphi) \right\} \Omega^2 + \frac{\varpi^4}{4c^2} \Omega^4 + \text{const}, \quad (3.1)$$

where X_0 , X_Ω , and $\hat{\beta}_\varphi$ are the gravitational potentials in the 1PN order which are obtained by solving the following Poisson equations:

$$\begin{aligned} \Delta \hat{P}_1 &= -4\pi G \rho \left(x_1 + \frac{R}{2} \right), \\ \Delta \hat{P}_2 &= -4\pi G \rho x_2, \\ \Delta X_0 &= 4\pi G \rho \left(\varepsilon + 2U + \frac{3P}{\rho} \right), \\ \Delta X_\Omega &= 8\pi G \rho \varpi^2, \end{aligned} \quad (3.2)$$

and

$$\begin{aligned} \hat{\beta}_\varphi &= - \left[\frac{7}{2} \left\{ \left(x_1 + \frac{R}{2} \right) \hat{P}_1 + x_2 \hat{P}_2 \right\} \right. \\ &\quad \left. + \frac{1}{2} \left\{ \left(x_1 + \frac{R}{2} \right)^2 \hat{P}_{2,2} + x_2^2 \hat{P}_{1,1} - \left(x_1 + \frac{R}{2} \right) x_2 (\hat{P}_{1,2} + \hat{P}_{2,1}) \right\} \right]. \end{aligned} \quad (3.3)$$

Note that in the incompressible case, $\varepsilon = 0$ and $\rho = \text{constant}$. Thus, the left hand-side of Eq. (3.1) is

$$\frac{P}{\rho} - \frac{1}{2c^2} \left(\frac{P}{\rho} \right)^2. \quad (3.4)$$

In the 1PN approximation, we have conserved quantities such as the conserved mass M_* , the energy E , and the angular momentum J which are written as^(27) 11)

$$M_* = \int \rho_* d^3x = \int \rho \left\{ 1 + \frac{1}{c^2} \left(\frac{v^2}{2} + 3U \right) \right\} d^3x, \quad (3.5)$$

$$\begin{aligned} E &= \int \rho \left\{ \varepsilon + \frac{v^2}{2} - \frac{1}{2} U \right. \\ &\quad \left. + \frac{1}{c^2} \left(\frac{5}{8} v^4 + \frac{5}{2} v^2 U + \frac{1}{2} \hat{\beta}_\varphi \Omega^2 + \varepsilon v^2 + \frac{P}{\rho} v^2 + 2\varepsilon U - \frac{5}{2} U^2 \right) \right\} d^3x, \end{aligned} \quad (3.6)$$

$$J = \int \rho \left[v_\varphi \left\{ 1 + \frac{1}{c^2} \left(v^2 + 6U + \varepsilon + \frac{P}{\rho} \right) \right\} + \frac{\hat{\beta}_\varphi \Omega}{c^2} \right] d^3x. \quad (3.7)$$

M_* conserves throughout the whole evolution of the system even if there exists a dissipation process such as the emission of GWs. Thus, in the case when we consider a sequence of a constant M_* , it may be regarded as an evolution sequence of the system.

Our purpose is to calculate the 1PN correction of the angular velocity, the energy and the angular momentum for corotating binary. To get the solution in the Newtonian order, we solve Eq. (2.15) with $\Lambda = 0$ using the angular velocity

$$\Omega^2 = \frac{2GM}{R^3} + \frac{18GI_{11}}{R^5} \equiv \Omega_N^2. \quad (3.8)$$

In the 1PN approximation, we can expect that the following types of quantities will be the main terms of the angular velocity in the 1PN order:

$$\sim \frac{GM}{R^3} \times \frac{GM}{a_0 c^2}, \quad \sim \frac{GM}{R^3} \times \frac{GM}{Rc^2}, \quad \sim \frac{GMa_0^2}{R^5} \times \frac{GM}{a_0 c^2} \quad \text{and} \quad \sim \frac{GMa_0^2}{R^5} \times \frac{GM}{Rc^2}, \quad (3.9)$$

where a_0 is a typical radius of the star and we use the relation $\mathcal{I}_{11} \sim Ma_0^2$. We will derive the details of four types of terms shown above in the correction of the energy and the angular momentum neglecting the effect of higher multipole terms.

As shown in Ref. 12), the neglect of the higher multipole terms brings us a great advantage so that we can regard each star of the binary as an ellipsoid whose shape is the same as that in the Newtonian order. This is because the deformation is induced by higher order effect of R^{-1} . Hence, we hereafter perform calculation setting density profile of each star as an ellipsoid of its axial length a_1 , a_2 and a_3 .

3.2. Gravitational potentials

As we did for the Newtonian potential U , we decompose PN gravitational potentials into two parts; one is the contribution from star 1 and the other is from star 2. In the following, we denote the former part as $\phi^{1 \rightarrow 1}$, and the latter one as $\phi^{2 \rightarrow 1}$, where ϕ denotes one of the potentials. We also define $\phi^{1 \rightarrow 2}$ and $\phi^{2 \rightarrow 2}$ as the contribution from star 1 to 2 and star 2 itself, respectively.

3.2.1. X_0

As we mentioned above, the 1PN potentials are divided into two parts as $X_0 = X_0^{1 \rightarrow 1} + X_0^{2 \rightarrow 1}$, and we consider them separately.

- Contribution from star 1

$X_0^{1 \rightarrow 1}$ is derived from the Poisson equation¹¹⁾

$$\Delta X_0^{1 \rightarrow 1} = 4\pi G\rho \left[2\pi G\rho \left(A_0 - \sum_l A_l x_l^2 \right) + \frac{3P_0}{\rho} \left(1 - \sum_l \frac{x_l^2}{a_l^2} \right) + 2U^{2 \rightarrow 1} \right], \quad (3.10)$$

and the solution becomes

$$X_0^{1 \rightarrow 1} = -\alpha_0 U^{1 \rightarrow 1} + \alpha_1 D_1 + \sum_l \eta_l D_l - \frac{M}{R^3} (2D_{11} - D_{22} - D_{33}) - \frac{M}{R^4} (-2D_{111} + 3D_{122} + 3D_{133}), \quad (3.11)$$

where

$$\alpha_0 = 2\pi G\rho A_0 + \frac{3P_0}{\rho} + \frac{2GM}{R} + \frac{3G\mathcal{I}_{11}}{R^3}, \quad (3.12)$$

$$\alpha_1 = \frac{2GM}{R^2} + \frac{9G\mathcal{I}_{11}}{R^4}, \quad (3.13)$$

$$\eta_l = 2\pi G\rho A_l + \frac{3P_0}{\rho a_l^2}. \quad (3.14)$$

D_i , D_{ii} , and D_{1ii} are the solutions of equations

$$\Delta D_i = -4\pi G\rho x_i, \quad (3.15)$$

$$\Delta D_{ii} = -4\pi G\rho x_i^2, \quad (3.16)$$

$$\Delta D_{1ii} = -4\pi G\rho x_1 x_i^2, \quad (3.17)$$

and the solutions at star 1 are¹⁸⁾

$$D_i = \pi G\rho a_i^2 \left(A_i - \sum_l A_{il} x_l^2 \right) x_i, \quad (3.18)$$

$$D_{ii} = \pi G\rho \left[a_i^4 \left(A_{ii} - \sum_l A_{iil} x_l^2 \right) x_i^2 + \frac{1}{4} a_i^2 \left(B_i - 2 \sum_l B_{il} x_l^2 + \sum_l \sum_m B_{ilm} x_l^2 x_m^2 \right) \right], \quad (3.19)$$

$$D_{111} = \pi G\rho \left[a_1^6 \left(A_{111} - \sum_l A_{111l} x_l^2 \right) x_1^3 + \frac{3}{4} a_1^4 \left(B_{11} - 2 \sum_l B_{11l} x_l^2 + \sum_l \sum_m B_{11lm} x_l^2 x_m^2 \right) x_1 \right], \quad (3.20)$$

$$D_{1ii} = \pi G\rho \left[a_1^2 a_i^4 \left(A_{1ii} - \sum_l A_{1iil} x_l^2 \right) x_1 x_i^2 + \frac{1}{4} a_1^2 a_i^2 \left(B_{1i} - 2 \sum_l B_{1il} x_l^2 + \sum_l \sum_m B_{1ilm} x_l^2 x_m^2 \right) x_1 \right], \quad (3.21)$$

where $B_{ijk\dots}$ are index symbols defined by Chandrasekhar.¹⁸⁾

- Contribution from star 2

The equation for $X_0^{2 \rightarrow 1}$ is

$$\Delta X_0^{2 \rightarrow 1} = 4\pi G\rho \left[2\pi G\rho \left(A_0 - \sum_l A_l y_l^2 \right) + \frac{3P_0}{\rho} \left(1 - \sum_l \frac{y_l^2}{a_l^2} \right) + 2U^{1 \rightarrow 2} \right], \quad (3.22)$$

where $y_1 = -(x_1 + R)$, $y_2 = x_2$ and $y_3 = x_3$. The solution is expressed as

$$X_0^{2 \rightarrow 1} = -\alpha_0 U^{2 \rightarrow 1} - \alpha_1 D_1^{2 \rightarrow 1} + \sum_l \eta_l D_{ll}^{2 \rightarrow 1} - \frac{M}{R^3} \left(2D_{11}^{2 \rightarrow 1} - D_{22}^{2 \rightarrow 1} - D_{33}^{2 \rightarrow 1} \right), \quad (3.23)$$

where $D_{ij\dots}^{2 \rightarrow 1}$ are calculated from the same equations as the case of $D_{ij\dots}$,¹⁸⁾ i.e.,

$$\Delta D_{ij\dots}^{2 \rightarrow 1} = -4\pi G\rho y_i y_j \dots \quad (3.24)$$

The solutions of $D_{ij\dots}^{2 \rightarrow 1}$ are

$$D_1^{2 \rightarrow 1} = \frac{GI_{11}}{R^2} \left(1 - \frac{2x_1}{R} + \frac{6x_1^2 - 3x_2^2 - 3x_3^2}{2R^2} + O(R^{-3}) \right), \quad (3.25)$$

$$D_2^{2 \rightarrow 1} = \frac{GI_{22}}{R^2} \left(\frac{x_2}{R} - \frac{3x_1x_2}{R^2} + O(R^{-3}) \right), \quad (3.26)$$

$$D_{ii}^{2 \rightarrow 1} = \frac{GI_{ii}}{R} \left(1 - \frac{x_1}{R} + \frac{2x_1^2 - x_2^2 - x_3^2}{2R^2} + \frac{-2x_1^3 + 3x_1(x_2^2 + x_3^2)}{2R^3} + O(R^{-4}) \right) \\ + \frac{3GI_{ii11}}{2R^3} \left(1 - \frac{3x_1}{R} + O(R^{-2}) \right), \quad (3.27)$$

where

$$I_{ii11} = I_{ii11} - \frac{1}{3} \sum_l I_{iill}. \quad (3.28)$$

3.2.2. X_Ω

- Contribution from star 1

The equation for $X_\Omega^{1 \rightarrow 1}$ is

$$\Delta X_\Omega^{1 \rightarrow 1} = 8\pi G\rho \left(x_1^2 + x_2^2 + Rx_1 + \frac{R^2}{4} \right). \quad (3.29)$$

Then the solution is

$$X_\Omega^{1 \rightarrow 1} = -2 \left(D_{11} + D_{22} + RD_1 + \frac{R^2}{4} U^{1 \rightarrow 1} \right). \quad (3.30)$$

- Contribution from star 2

The equation $X_\Omega^{2 \rightarrow 1}$ may be written as

$$\Delta X_\Omega^{2 \rightarrow 1} = 8\pi G\rho \left(y_1^2 + y_2^2 - Ry_1 + \frac{R^2}{4} \right). \quad (3.31)$$

Then, using $D_{ij \dots}^{2 \rightarrow 1}$, the solution is easily derived as

$$X_\Omega^{2 \rightarrow 1} = -2 \left(D_{11}^{2 \rightarrow 1} + D_{22}^{2 \rightarrow 1} - RD_1^{2 \rightarrow 1} + \frac{R^2}{4} U^{2 \rightarrow 1} \right), \quad (3.32)$$

$$= -\frac{R^2}{2} U^{2 \rightarrow 1} - \frac{2GI_{11}}{R^2} x_1 - \frac{2GI_{22}}{R} \left(1 - \frac{x_1}{R} \right). \quad (3.33)$$

3.2.3. $\hat{\beta}_\varphi$

$\hat{\beta}_\varphi$ is obtained from \hat{P}_1 and \hat{P}_2 which satisfy,

$$\Delta \hat{P}_1 = -4\pi G\rho \left(x_1 + \frac{R}{2} \right), \quad (3.34)$$

$$\Delta \hat{P}_2 = -4\pi G\rho x_2. \quad (3.35)$$

\hat{P}_i is also written as $\hat{P}_i^{1 \rightarrow 1} + \hat{P}_i^{2 \rightarrow 1}$, where

$$\hat{P}_1^{1 \rightarrow 1} = D_1 + \frac{R}{2} U^{1 \rightarrow 1}, \quad (3.36)$$

$$\hat{P}_2^{1 \rightarrow 1} = D_2 \quad (3.37)$$

and

$$\hat{P}_1^{2 \rightarrow 1} = D_1^{2 \rightarrow 1} - \frac{R}{2} U^{2 \rightarrow 1}, \quad (3.38)$$

$$\hat{P}_2^{2 \rightarrow 1} = D_2^{2 \rightarrow 1}. \quad (3.39)$$

3.3. The Post-Newtonian angular velocity and definition of mass and center of mass

As in the Newtonian case, the orbital angular velocity in the 1PN order is also derived using the first TV equation as

$$\begin{aligned} 0 = \int \frac{\partial P}{\partial x_1} d^3x &= \int \rho U_{,1} d^3x + \frac{R}{2} M \Omega^2 + \frac{1}{c^2} \left[- \int \rho X_{0,1} d^3x \right. \\ &\quad \left. + \Omega_N^2 \int \rho \left(2\varpi^2 U_{,1} + 4x_1 U + 2RU - X_{\Omega,1} + \beta_{\varphi,1} \right) d^3x \right. \\ &\quad \left. + \Omega_N^4 \left(\frac{R}{2} (3I_{11} + I_{22}) + \frac{MR^3}{8} \right) \right], \end{aligned} \quad (3.40)$$

where “ k ” denotes the partial derivative with respect to x_k . Since all the gravitational potentials can be written as the polynomial form of x_k , we can immediately perform the integral shown above and obtain Ω^2 as

$$\begin{aligned} \Omega^2 &= \frac{2GM}{R^3} \left[1 + \frac{G}{c^2} \left\{ 2\pi\rho A_0 - \frac{9M}{4R} - \frac{M}{10R^3} (28a_1^2 - 14a_2^2 - 9a_3^2) + O(R^{-4}) \right\} \right] \\ &\quad + \frac{18G\mathcal{I}_{11}}{R^5} \left(1 + \frac{28}{15c^2} \pi G \rho A_0 + O(R^{-2}) \right), \end{aligned} \quad (3.41)$$

where we make use of the relations $A_0 = \sum_l A_l a_l^2$ and Eqs. (2.15) with $\Lambda = 0$ to simplify the expression.

Next, we discuss the mass of the system and definition of the center of mass for each star. This is because there are several definitions of them in the 1PN approximation, and we should clarify the difference between the similar ones.

First, we consider the conserved mass which is defined as

$$\begin{aligned} M_* &= \int d^3x \rho \left[1 + \frac{1}{c^2} \left(\frac{v^2}{2} + 3U \right) \right] \\ &= M \left[1 + \frac{G}{c^2} \left(\frac{13M}{4R} + \frac{12\pi\rho A_0}{5} + \frac{M}{20R^3} (34a_1^2 - 11a_2^2 - 15a_3^2) + O(R^{-5}) \right) \right]. \end{aligned} \quad (3.42)$$

Using M_* , Ω^2 becomes

$$\begin{aligned} \Omega^2 &= \frac{2GM_*}{R^3} \left[1 + \frac{G}{c^2} \left\{ -\frac{2\pi\rho A_0}{5} - \frac{11M_*}{2R} - \frac{M_*}{20R^3} (90a_1^2 - 39a_2^2 - 33a_3^2) \right\} + O(R^{-4}) \right] \\ &\quad + \frac{18G(\mathcal{I}_{11})_*}{R^5} \left[1 + \frac{G}{c^2} \left\{ -\frac{8}{15} \pi \rho A_0 - \frac{13M_*}{4R} + O(R^{-2}) \right\} \right], \end{aligned} \quad (3.43)$$

where $(\mathcal{I}_{11})_* = M_* \mathcal{I}_{11}/M$. Thus, Ω^2 looks as if it depends on the internal structure of the star even in the limit of $a_i/R \rightarrow 0$. Since we believe that in the EOM for the point particle, the quantities depending on the internal structure does not appear, M_* is not desirable to describe the EOM for the point particle. Instead, in the case when the EOM is derived, one usually adopts the PPN mass²⁸⁾ defined as

$$\begin{aligned} M_{\text{PPN}} &= \int d^3x \rho \left[1 + \frac{1}{c^2} \left(\frac{v^2}{2} + 3U - \frac{1}{2}U_{\text{self}} + \frac{v_{\text{self}}^2}{2} \right) \right] \\ &= M \left[1 + \frac{G}{c^2} \left(\frac{13M}{4R} + 2\pi\rho A_0 + \frac{M}{20R^3} (38a_1^2 - 7a_2^2 - 15a_3^2) + O(R^{-5}) \right) \right], \end{aligned} \quad (3.44)$$

where U_{self} and v_{self} are the self-gravity part of the Newtonian potential and the spin velocity of each star. When we rewrite Eq. (3.41) using the PPN mass, the orbital angular velocity does not depend on the internal structure of the star and it agrees with that for the point particle²⁹⁾ in the limit of $a_i/R \rightarrow 0$ as

$$\begin{aligned} \Omega^2 &= \frac{2GM_{\text{PPN}}}{R^3} \left[1 + \frac{G}{c^2} \left\{ -\frac{11M_{\text{PPN}}}{2R} - \frac{M_{\text{PPN}}}{20R^3} (94a_1^2 - 35a_2^2 - 33a_3^2) + O(R^{-4}) \right\} \right] \\ &\quad + \frac{18G(\mathcal{I}_{11})_{\text{PPN}}}{R^5} \left[1 + \frac{G}{c^2} \left\{ -\frac{2}{15}\pi\rho A_0 - \frac{13M_{\text{PPN}}}{4R} + O(R^{-2}) \right\} \right], \end{aligned} \quad (3.45)$$

where $(\mathcal{I}_{11})_{\text{PPN}} = M_{\text{PPN}} \mathcal{I}_{11}/M$. Thus, when we compare the present results with the point particle calculations, we should use the PPN mass. In the present case, however, M_{PPN} is not a conserved quantity although M_* is. When we consider a sequence of equilibrium configurations as an evolutionary sequence, we should fix M_* .

Next, we consider the definition of the center of mass for each star. In the PPN formalism, it is defined as²⁸⁾

$$x_{\text{PPN}}^i = \frac{1}{M_{\text{PPN}}} \int d^3x \rho x^i \left[1 + \frac{1}{c^2} \left(\frac{v^2}{2} + 3U - \frac{1}{2}U_{\text{self}} + \frac{v_{\text{self}}^2}{2} \right) \right]. \quad (3.46)$$

x_1 coordinate of the center of mass for star 1 deviates from 0 to

$$\frac{G}{c^2} \left(-\frac{2Ma_1^2}{5R^2} + O(R^{-4}) \right). \quad (3.47)$$

Thus, in the PPN formalism, the following orbital separation should be used;

$$R_{\text{PPN}} = R \left[1 + \frac{G}{c^2} \left\{ -\frac{4Ma_1^2}{5R^3} + O(R^{-5}) \right\} \right]. \quad (3.48)$$

It is worth noting that when we define the center of mass by the conserved mass as

$$x_*^i = \frac{1}{M_*} \int d^3x \rho_* x^i, \quad (3.49)$$

the result is the same up to $O(R^{-4})$. Thus, in this paper, we do not have to distinguish R_* from R_{PPN} . Even in the general case, the difference between R_* and R_{PPN} is expected to be small.

Using R_* and/or R_{PPN} , Ω^2 is rewritten as

$$\begin{aligned} \Omega^2 = \frac{2GM_*}{R_*^3} & \left[1 + \frac{G}{c^2} \left\{ -\frac{2\pi\rho A_0}{5} - \frac{11M_*}{2R_*} \right. \right. \\ & \left. \left. - \frac{M_*}{20R_*^3} (138a_1^2 - 39a_2^2 - 33a_3^2) + O(R_*^{-4}) \right\} \right] \\ & + \frac{18G(\mathcal{I}_{11})_*}{R_*^5} \left[1 + \frac{G}{c^2} \left\{ -\frac{8}{15}\pi\rho A_0 - \frac{13M_*}{4R_*} + O(R_*^{-2}) \right\} \right], \end{aligned} \quad (3.50)$$

or

$$\begin{aligned} \Omega^2 = \frac{2GM_{\text{PPN}}}{R_{\text{PPN}}^3} & \left[1 + \frac{G}{c^2} \left\{ -\frac{11M_{\text{PPN}}}{2R_{\text{PPN}}} \right. \right. \\ & \left. \left. - \frac{M_{\text{PPN}}}{20R_{\text{PPN}}^3} (142a_1^2 - 35a_2^2 - 33a_3^2) + O(R_{\text{PPN}}^{-4}) \right\} \right] \\ & + \frac{18G(\mathcal{I}_{11})_{\text{PPN}}}{R_{\text{PPN}}^5} \left[1 + \frac{G}{c^2} \left\{ -\frac{2}{15}\pi\rho A_0 - \frac{13M_{\text{PPN}}}{4R_{\text{PPN}}} + O(R_{\text{PPN}}^{-2}) \right\} \right]. \end{aligned} \quad (3.51)$$

Here, we should note that the effect of the spin-orbit coupling terms will appear in Ω^2 from $O(R_{\text{PPN}}^{-6})$.³⁰⁾ According to the 1PN study, it becomes

$$\Omega^2 = \frac{2GM_{\text{PPN}}}{R_{\text{PPN}}^3} \left[1 - \frac{2GM_{\text{PPN}}}{c^2 R_{\text{PPN}}^3} (a_1^2 + a_2^2) \right], \quad (3.52)$$

where we omit other terms which are not related to this discussion. Eq. (3.52) shows that the terms of $O(R_{\text{PPN}}^{-6})$ in Eq. (3.51) cannot be explained only by the spin-orbit coupling term. This will mean that there appears a new effect, say the 1PN quadrupole one, in Eq. (3.51).^{*)}

3.4. The energy and the angular momentum

3.4.1. The Total Energy

The 1PN total energy is calculated from $E = E_{\text{N}}^{\text{def}} + E_{\text{PN}}^{\text{def}}/c^2$, where^{27) 11)}

$$E_{\text{N}}^{\text{def}} = \int \rho \left(\frac{1}{2}v^2 - \frac{1}{2}U \right) d^3x, \quad (3.53)$$

$$E_{\text{PN}}^{\text{def}} = \int \rho \left(\frac{5}{8}v^4 + \frac{5}{2}v^2U + \frac{P}{\rho}v^2 - \frac{5}{2}U^2 + \frac{1}{2}\hat{\beta}_\varphi\Omega^2 \right) d^3x. \quad (3.54)$$

^{*)} In this paper, we use the PPN mass in order to compare the angular velocity with that of the point particle case. However, the PPN mass is useful only for the point particle case because it does not conserve if we take into account the tidal forces on each star of binary. In the context of this paper, we have to use the mass which is valid even if the tidal forces exist. Unfortunately, no one has proposed such a mass as far as we know.

For the 1PN corotating binary, they become

$$\begin{aligned}
E_N^{\text{def}} &= M \left[-\frac{4\pi G\rho A_0}{5} + \frac{\Omega^2}{5}(a_1^2 + a_2^2) + \frac{R^2\Omega^2}{4} - \frac{GM}{R} - \frac{3G\mathcal{I}_{11}}{R^3} + O(R^{-5}) \right], \\
E_{\text{PN}}^{\text{def}} &= 2G^2M \left[-\frac{34}{21}(\pi\rho A_0)^2 - \frac{11M\pi\rho A_0}{3R} - \frac{7M^2}{32R^2} \right. \\
&\quad \left. + \frac{M\pi\rho A_0}{R^3} \left\{ \frac{68}{105}(a_1^2 + a_2^2) - \frac{61}{7} \frac{\mathcal{I}_{11}}{M} \right\} \right. \\
&\quad \left. + \frac{M^2}{240R^4}(302a_1^2 + 59a_2^2 - 209a_3^2) + O(R^{-5}) \right]. \quad (3.55)
\end{aligned}$$

If we substitute Ω^2 into the above formulas, E may be rewritten as $E_N + E_{\text{PN}}/c^2$ where

$$\begin{aligned}
E_N &= M \left[-\frac{4\pi G\rho A_0}{5} - \frac{GM}{2R} + \frac{3G\mathcal{I}_{11}}{2R^3} + \frac{\Omega_N^2}{5}(a_1^2 + a_2^2) + O(R^{-5}) \right], \quad (3.56) \\
E_{\text{PN}} &= 2G^2M \left[-\frac{34}{21}(\pi\rho A_0)^2 - \frac{19M\pi\rho A_0}{6R} - \frac{25M^2}{32R^2} \right. \\
&\quad \left. + \frac{M\pi\rho A_0}{R^3} \left\{ \frac{22}{21}(a_1^2 + a_2^2) - \frac{158}{35} \frac{\mathcal{I}_{11}}{M} \right\} \right. \\
&\quad \left. + \frac{M^2}{240R^4}(26a_1^2 + 35a_2^2 - 155a_3^2) + O(R^{-5}) \right]. \quad (3.57)
\end{aligned}$$

3.4.2. The Total Angular Momentum

We can calculate the 1PN total angular momentum from $J = J_N^{\text{def}} + J_{\text{PN}}^{\text{def}}/c^2$, where^{27) 11)}

$$J_N^{\text{def}} = \int \rho v_\varphi d^3x, \quad (3.58)$$

$$J_{\text{PN}}^{\text{def}} = \int \rho \left[v_\varphi \left(v^2 + 6U + \frac{P}{\rho} \right) + \hat{\beta}_\varphi \Omega \right] d^3x, \quad (3.59)$$

and $v_\varphi = \Omega\varpi^2$. For the PN corotating binary, they become

$$\begin{aligned}
J_N^{\text{def}} &= 2M\Omega \left(\frac{R^2}{4} + \frac{a_1^2 + a_2^2}{5} \right), \\
J_{\text{PN}}^{\text{def}} &= GM\Omega_N \left[R^2\pi\rho A_0 + 5RM + \frac{164}{105}\pi\rho A_0(a_1^2 + a_2^2) \right. \\
&\quad \left. + \frac{M}{10R}(20a_1^2 + 15a_2^2 - 11a_3^2) + O(R^{-2}) \right]. \quad (3.60)
\end{aligned}$$

If we substitute Ω^2 into the above formulas, J may be rewritten as $J_N + J_{\text{PN}}/c^2$ where

$$J_N = 2M\Omega_N \left(\frac{R^2}{4} + \frac{a_1^2 + a_2^2}{5} \right), \quad (3.61)$$

$$J_{\text{PN}} = GM\Omega_N \left[\frac{3}{2}R^2\pi\rho A_0 + \frac{71}{16}RM + \frac{\pi\rho A_0}{1050}(2018a_1^2 + 2081a_2^2 + 21a_3^2) \right. \\ \left. + \frac{M}{80R}(122a_1^2 + 85a_2^2 - 97a_3^2) + O(R^{-2}) \right]. \quad (3.62)$$

3.5. Construction of equilibrium sequences

To construct equilibrium sequences of 1PN corotating binary stars fixing M_* and ρ , we use the following method:

Step (1): Using Eqs. (2.15) with $\Lambda = 0$, we numerically calculate equilibrium sequences in the Newtonian order. Up to this stage, α_2 , α_3 , and $\tilde{R} = R/a_1$ are determined.

Step (2): a_1 is determined from the condition $M_* = \text{constant}$ using Eq. (3.42):

$$a_1^3 = \frac{3M_*}{4\pi\rho\alpha_2\alpha_3} \left[1 - \frac{\pi G\rho}{c^2} \left(\frac{3M_*}{4\pi\rho\alpha_2\alpha_3} \right)^{2/3} \left(\frac{12\tilde{A}_0}{5} + \frac{13\alpha_2\alpha_3}{3\tilde{R}} + \frac{\alpha_2\alpha_3}{15\tilde{R}^3}(34 - 11\alpha_2^2 - 15\alpha_3^2) \right) \right]. \quad (3.63)$$

Step (3): After substituting Eq. (3.63) into Eqs. (3.41), (3.55), and (3.60), we rewrite the 1PN expressions for the orbital angular velocity, the energy and the angular momentum as

$$\tilde{\Omega}^2 \equiv \frac{\Omega^2}{\Omega_*^2} = \tilde{\Omega}_N^2 + \frac{GM_*}{c^2 a_*} \tilde{\Omega}_{\text{PN}}^2, \quad (3.64)$$

$$\tilde{E} \equiv \frac{E}{(GM_*^2/a_*)} = \tilde{E}_N + \frac{GM_*}{c^2 a_*} \tilde{E}_{\text{PN}}, \quad (3.65)$$

$$\tilde{J} \equiv \frac{J}{(GM_*^3 a_*)^{1/2}} = \tilde{J}_N + \frac{GM_*}{c^2 a_*} \tilde{J}_{\text{PN}}, \quad (3.66)$$

where

$$a_* = \left(\frac{3M_*}{4\pi\rho} \right)^{1/3}, \quad (3.67)$$

$$\tilde{\Omega}_N^2 = \alpha_2\alpha_3 \left[\frac{2}{\tilde{R}^3} + \frac{6}{5\tilde{R}^5}(2 - \alpha_2^2 - \alpha_3^2) \right], \quad (3.68)$$

$$\tilde{\Omega}_*^2 = \frac{GM_*}{a_*^3}, \quad (3.69)$$

$$\tilde{\Omega}_{\text{PN}}^2 = (\alpha_2\alpha_3)^{4/3} \left[\frac{3}{\tilde{R}^3} \frac{\tilde{A}_0}{\alpha_2\alpha_3} - \frac{9}{2\tilde{R}^4} + \frac{42}{25\tilde{R}^5} \frac{\tilde{A}_0}{\alpha_2\alpha_3} (2 - \alpha_2^2 - \alpha_3^2) \right. \\ \left. - \frac{1}{5\tilde{R}^6} (28 - 14\alpha_2^2 - 9\alpha_3^2) \right], \quad (3.70)$$

$$\tilde{E}_N = (\alpha_2\alpha_3)^{1/3} \left[-\frac{3}{5} \frac{\tilde{A}_0}{\alpha_2\alpha_3} - \frac{1}{2\tilde{R}} + \frac{1}{10\tilde{R}^3} (2 - \alpha_2^2 - \alpha_3^2) + \frac{\tilde{\Omega}_N^2}{5\alpha_2\alpha_3} (1 + \alpha_2^2) \right], \quad (3.71)$$

$$\tilde{E}_{\text{PN}} = (\alpha_2\alpha_3)^{2/3} \left[-\frac{3}{140} \left(\frac{\tilde{A}_0}{\alpha_2\alpha_3} \right)^2 + \frac{55}{48\tilde{R}^2} + \frac{1}{700\tilde{R}^3} \frac{\tilde{A}_0}{\alpha_2\alpha_3} (398 + 401\alpha_2^2 + \alpha_3^2) - \frac{1}{120\tilde{R}^4} (194 + 215\alpha_2^2 + 165\alpha_3^2) \right], \quad (3.72)$$

$$\tilde{J}_N = 2(\alpha_2\alpha_3)^{-1/6} \left[\frac{\tilde{\Omega}_N^2}{\alpha_2\alpha_3} \right]^{1/2} \left(\frac{\tilde{R}^2}{4} + \frac{1 + \alpha_2^2}{5} \right), \quad (3.73)$$

$$\tilde{J}_{\text{PN}} = (\alpha_2\alpha_3)^{1/6} \left[\frac{\tilde{\Omega}_N^2}{\alpha_2\alpha_3} \right]^{1/2} \left[-\frac{3}{8} \tilde{R}^2 \frac{\tilde{A}_0}{\alpha_2\alpha_3} + \frac{83}{48} \tilde{R} + \frac{1}{1400} \frac{\tilde{A}_0}{\alpha_2\alpha_3} (338 + 401\alpha_2^2 + 21\alpha_3^2) - \frac{1}{240\tilde{R}} (494 + 155\alpha_2^2 + 141\alpha_3^2) \right]. \quad (3.74)$$

Then, using the numerical value of α_2 , α_3 , and \tilde{R} determined at step (1), we calculate the sequence of the angular velocity, the energy and the angular momentum as functions of the orbital separation.

We repeat this procedure changing the mean radius of each star a_* . Once a sequence is obtained, we search the minimum point of the energy. If we find it, we call it the ISCCO. The 1PN approximation is valid only for small $C_s \equiv GM_*/c^2 a_*$, i.e., the characteristic value of the compactness of each star. Thus, we hereafter show results only for small C_s .

In Figs.6(a) and (b), we show $\tilde{E} = E/(GM_*^2/a_*)$ and $\tilde{J} = J/(GM_*^3 a_*)^{1/2}$ as functions of Ω/Ω_* . The figures show the important fact that the angular velocity at the ISCCO increases approximately in proportion to C_s .

In Fig.7, we show $\tilde{\Omega} = \Omega/\Omega_*$ at the ISCCO as a function of C_s . We show $\tilde{\Omega}$ at the energy minimum as well as that at the angular momentum minimum. The figure indicates that two minima are almost coincident, but slightly different. We guess that this disagreement is due to the neglect of the effect from the higher multipole deformation. In any case, we may expect that the ISCCO locates near two minima. Fig.7 clearly shows that the orbital angular velocity at the ISCCO increases almost linearly with increase of C_s as

$$\Omega_{\text{ISCCO}} = \Omega_{N:\text{ISCCO}} \left(1 + C_{\text{PN}}(n) C_s \right), \quad (3.75)$$

where $C_{\text{PN}}(n)$ is a constant which depends on the EOS (see next section) and for the incompressible case, $C_{\text{PN}}(0) \simeq 0.5$.

We briefly argue the meaning of the result for Ω_{ISCCO} using Eq. (3.72). In Eq. (3.72), there appear mainly two kinds of effects in the first and second terms,

respectively: The first term concerns the internal structure of each star and denotes that each star is forced to be compact due to the 1PN gravity because of its negative definite character. Thus, the first term acts as the stabilization because the tidal effect is less important in the case when the star becomes compact. On the other hand, the second term concerns the gravity acting between two stars because it exists in the limit $a_1, a_2, a_3 \rightarrow 0$. This term tends to act as destabilization of circular orbits because of its dependence of \tilde{R} ($O(\tilde{R}^{-2})$) and its positive definite character. In this way, there exist two opposite effects in the 1PN corrections, and the present result shows that the former effect dominates over the latter one.

§4. First post Newtonian study: Compressible case

For compressible stars, we can no longer solve the integrated form of the Euler equation analytically although we make approximate solutions assuming density profile of each star appropriately.^{13) 31)} To obtain accurate equilibrium states, we need numerical calculation. In this section, we show numerical results for sequences of 1PN corotating equilibrium binaries obtained by solving the integrated form of the Euler equation as well as the Poisson equations for the gravitational potentials. We use a numerical method which is developed in previous papers.¹¹⁾

In the compressible case, the integrated form of the Euler equation for uniformly rotating fluid is

$$\begin{aligned} & K(n+1)\rho^{1/n} - \frac{1}{2c^2} \left(K(n+1)\rho^{1/n} \right)^2 \\ &= U - \frac{X_0}{c^2} + \left\{ \frac{\varpi^2}{2} + \frac{1}{c^2} \left(2\varpi^2 U - X_\Omega + \hat{\beta}_\varphi \right) \right\} \Omega^2 + \frac{\varpi^4}{4c^2} \Omega^4 + \text{const}, \quad (4.1) \end{aligned}$$

where we assume the polytropic EOS, i.e.,

$$P = K\rho^{1+1/n} \quad \text{and} \quad \varepsilon = \frac{nP}{\rho}. \quad (4.2)$$

Hereafter, we set $n = 0.5, 0.75$ and 1 because real NSs will have $n = 0.5 \sim 1$.²²⁾ The gravitational potential in the 1PN order are obtained by solving Eqs. (3.2). The conserved mass, the energy, and the angular momentum are defined as Eqs. (3.5)-(3.7). Following a previous section, we hereafter show the angular velocity, the energy and the angular momentum in units of $\Omega_* \equiv (GM_*/a_*^3)^{1/2}$, GM_*^2/a_* and $(GM_*^3 a_*)^{1/2}$, where

$$\begin{aligned} a_* &= \left(\frac{KM_*}{2.524G} \right)^{1/5} && \text{for } n = 0.5, \\ &= \left(\frac{KM_*^{1/3}}{0.9960G} \right)^{1/3} && \text{for } n = 0.75, \\ &= \left(\frac{\pi K}{2G} \right)^{1/2} && \text{for } n = 1, \end{aligned}$$

$$(4.3)$$

We also define the center of mass for each star as

$$x_{1*} = \frac{1}{M_*} \int \rho_* x_1 d^3x, \quad (4.4)$$

and as a result, the orbital separation is defined to be $R_* = 2x_{1*}$. In numerical computation, sequences of equilibrium states are obtained fixing M_* and K .

First, we demonstrate that our numerical results are reliable by showing the relation between the orbital separation and the angular velocity. If we neglect the contribution from the quadrupole deformation of each star, the angular velocity in the 1PN approximation can be approximately expressed as^{28) 11)}

$$\Omega = \sqrt{\frac{GM_*}{R_*^3}} \left[1 + \frac{G}{c^2} \left(-\frac{3-n}{2(5-n)} \frac{M_*}{a_*} - \frac{11M_*}{8R_*} \right) \right]. \quad (4.5)$$

Numerical results should agree well with this analytic formula. In Fig.8, we show the relation between R_*/a_* and Ω/Ω_* for $n = 0.5$ and $C_s \equiv GM_*/a_*c^2 = 0$ (open circles), 0.0327 (filled circles) and 0.0654 (open squares) as examples. Dotted lines are drawn using Eq. (4.5) as counter parts of the numerical results. The figure shows that numerical results agree with the analytic formula well except for slight deviation caused by the deformation of each star.

In Figs.9, we show the energy and angular momentum as functions of Ω/Ω_* for sequences of $n = 0.5$ (a), 0.75(b) and 1(c). In Fig.9(a), open circles, filled circles, and open squares denotes sequences for $C_s = 0, 0.0327$ and 0.0654 , in Fig.9(b), they denote sequences for $C_s = 0, 0.02$ and 0.04 , and in Fig.9(c), they denote sequences for $C_s = 0, 0.0167$ and 0.0333 , respectively. It is shown that the minima of the energy and the angular momentum almost coincide, and Ω/Ω_* at those minima (i.e., ISCCO) increases with increase of C_s as in the incompressible case.

In figs.10, we show the orbital angular velocity at the ISCCO as a function of C_s for $n = 0.5$ (a), 0.75(b) and 1(c). It is found that as in the case $n = 0$, Ω_{ISCCO} almost linearly increases with increase of C_s as

$$\Omega_{\text{ISCCO}} = \Omega_{\text{N:ISCCO}} \left(1 + C_{\text{PN}}(n)C_s \right), \quad (4.6)$$

where $C_{\text{PN}}(0.5) \sim 1.1$, $C_{\text{PN}}(0.75) \sim 1.8$, and $C_{\text{PN}}(1) \sim 2.5$. Thus, not only $\Omega_{\text{N:ISCCO}}$, but also C_{PN} changes with the EOS, and for softer EOS, Ω_{ISCCO} sensitively increases with C_s because the 1PN effect of the self gravity is larger for the softer EOS.

The summary of §3 and §4 is as follows.

1. Ω_{ISCCO} increases with the increase of the 1PN GR correction.
This is because each star of the binary becomes compact due to the strong GR self-gravity and as a result, the tidal effect becomes less effective.
2. The feature mentioned at 1 is more remarkable for larger n , i.e., for softer EOS.
The reason for this behavior is that for softer EOS, each star has the larger central density and is susceptible to the GR correction.

These conclusions are obtained by analyzing equilibrium sequences of corotating binary. However, it seems that these features may not be very sensitive to the spin and circulation of each star because the above properties mainly originate from the change of the density profile due to the GR correction. Therefore, we may expect that the similar trend will hold for constant- C sequences although more investigation is needed for this point.

§5. GR orbital effects: Pseudo-Newtonian potential approach

In previous two sections, we investigated the stability of corotating binary in the 1PN approximation, and showed Ω_{ISCCO} increases with the increase of the GR correction. This may be viewed from another point. In the 1PN approximation ISCO does not exist in the point particle limit.³²⁾ Therefore with the increase of relativity parameter C_s , Ω_{ISCO} should increase since the increase of the relativity parameter means the way toward the point particle limit where the circular orbit exists for any radius. On the other hand, if we include the GR effect to the gravity acting between two stars in which ISCO exists even in the point particle limit but we do not include the self-gravity of each star, Ω_{ISCO} decreases compared with Ω_{ISCO} in the point particle limit. This seems to apparently disagree with the results in previous sections. In the following, we first review the result of the work by TN,¹⁴⁾ which is one of such studies. (We note that there is the other work by LW,¹⁵⁾ in which the qualitative features of the results are essentially the same as those by TN.) In the last subsection, we clarify the reason for this apparent disagreement. We will show that this disagreement simply comes from the difference of two treatments. We also suggest that if 1PN effect of the self-gravity is included in the formalism of TN, Ω_{ISCO} will increase from the results without the 1PN self-gravity effect.

5.1. Outline of method

Here, we consider the so called Roche-Riemann problem¹⁸⁾ as a model of a binary that consists of a finite size star (star 1) and a point-like gravity source (star 2). To mimic the GR potential between two stars in which circular orbits are unstable for small radii, we use the pseudo-Newtonian potential proposed by Paczyński and Wiita.³³⁾ Details of the method by TN are as follows.

First, we regard star 2 as a point-like star of mass m_2 and denote the gravitational potential by it as $V_2(r)$. To include the effects of general relativity phenomenologically, we adopt pseudo-Newtonian potential as $V_2(r)$ (see below). Then, as star 1, we adopt the incompressible and homogeneous ellipsoid of its axial length a_1 , a_2 and a_3 , mass m_1 and the density ρ_1 . The structure of star 1 is determined by the Newtonian hydrostatic equation. Thus, the self-gravity part of the gravitational potential V_1 is the same as that in Eq. (2.7).

5.2. Basic equations

We use the tensor virial method¹⁸⁾ to derive the equations necessary for determining the orbital angular velocity and for constructing equilibrium configurations of star 1. We choose the coordinate system such that the origin is at the center of

mass of star 1 and the x_1 -axis points to the center of mass of star 2 which is located at $(-R, 0, 0)$. The x_3 -axis is chosen to be the axis of the orbital rotation. In the frame of reference rotating with Ω , the hydrostatic equation of star 1 is written as

$$\begin{aligned} \rho_1 \sum_{j=1}^3 u_j \frac{\partial u_i}{\partial x_j} = & -\frac{\partial P}{\partial x_i} + \rho_1 \frac{\partial}{\partial x_i} \left[V_1 + V_2 + \frac{\Omega^2}{2} \left\{ \left(\frac{m_2 R}{m_1 + m_2} + x_1 \right)^2 + x_2^2 \right\} \right] \\ & + 2\rho_1 \Omega \sum_{l=1}^3 \epsilon_{il3} u_l, \end{aligned} \quad (5.1)$$

where u_i , P , and R are the internal velocity, the pressure, and the separation between two stars, respectively.

Following Chandrasekhar,¹⁸⁾ we expand the interaction potential V_2 in the power series of x_k up to the second order assuming $R \gg a_1, a_2$ and a_3 . We assume that the potential V_2 depends only on the distance r from the center of mass of star 2 as

$$V_2 = V_2(r), \quad (5.2)$$

where r is given by

$$r = \left\{ (R + x_1)^2 + x_2^2 + x_3^2 \right\}^{1/2}. \quad (5.3)$$

The expansion of $V_2(r)$ near the coordinate origin becomes

$$V_2 = (V_2)_0 + \left(\frac{\partial V_2}{\partial r} \right)_0 x_1 + \frac{1}{2} \left(\frac{\partial^2 V_2}{\partial r^2} \right)_0 x_1^2 + \frac{1}{2R} \left(\frac{\partial V_2}{\partial r} \right)_0 (x_2^2 + x_3^2), \quad (5.4)$$

where the subscript 0 denotes the derivatives at the origin of the coordinate. From the force balance at the center, we obtain the orbital angular velocity as

$$\frac{m_2 R}{m_1 + m_2} \Omega^2 = - \left(\frac{\partial V_2}{\partial r} \right)_0 (1 + \delta), \quad (5.5)$$

where δ is the quadrupole term of the interaction potential⁹⁾. If we take the Newtonian potential

$$V_2(r) = \frac{Gm_2}{r} \quad (5.6)$$

as an interaction potential, δ is written as

$$\delta = \frac{3}{10R^2} (2a_1^2 - a_2^2 - a_3^2). \quad (5.7)$$

Substituting Eqs. (5.4) and (5.5) into Eq. (5.1), we have

$$\begin{aligned} \rho_1 \sum_{j=1}^3 u_j \frac{\partial u_i}{\partial x_j} = & -\frac{\partial P}{\partial x_i} + \rho_1 \frac{\partial}{\partial x_i} \left[V_1 - \delta \left(\frac{\partial V_2}{\partial r} \right)_0 x_1 + \frac{1}{2} \Omega^2 (x_1^2 + x_2^2) + \frac{1}{2} \left(\frac{\partial^2 V_2}{\partial r^2} \right)_0 x_1^2 \right. \\ & \left. + \frac{1}{2R} \left(\frac{\partial V_2}{\partial r} \right)_0 (x_2^2 + x_3^2) \right] + 2\rho_1 \Omega \sum_{l=1}^3 \epsilon_{il3} u_l. \end{aligned} \quad (5.8)$$

Multiplying x_j to Eq. (5·8) and integrating over the volume of star 1, we have

$$0 = 2T_{ij} + W_{ij} + \left\{ \Omega^2 + \left(\frac{\partial^2 V_2}{\partial r^2} \right)_0 \right\} \delta_{1i} I_{1j} + \left\{ \Omega^2 + \frac{1}{R} \left(\frac{\partial V_2}{\partial r} \right)_0 \right\} \delta_{2i} I_{2j} + \frac{1}{R} \left(\frac{\partial V_2}{\partial r} \right)_0 \delta_{3i} I_{3j} + 2\Omega \sum_{l=1}^3 \epsilon_{il3} \int \rho_1 u_l x_j d^3x + \delta_{ij} \Pi, \quad (5-9)$$

where

$$T_{ij} \equiv \frac{1}{2} \int \rho_1 u_i u_j d^3x : \text{Kinetic energy tensor}, \quad (5-10)$$

$$W_{ij} \equiv \int \rho_1 \frac{\partial V_1}{\partial x_i} x_j d^3x : \text{Potential energy tensor}, \quad (5-11)$$

$$I_{ij} \equiv \int \rho_1 x_i x_j d^3x : \text{Moment of inertia tensor} \quad (5-12)$$

and

$$\Pi \equiv \int P d^3x. \quad (5-13)$$

In Eq. (5·9) there appear no terms related to δ . Since it is possible to take the coordinate system moving with a constant velocity, the term proportional to δ in Eq. (5·8) can be vanished. Equation (5·9) is the basic equation to construct equilibrium configurations of star 1. Note that in this model, the GR effects generated by star 2 are included in the orbital angular velocity and the tidal potential at star 1.

Using Eqs. (2·7), (2·10), and (2·11) for the self-gravity part of the potential V_1 , the pressure P , and the internal velocity u_i , respectively, we obtain three equations from Eq. (5·9);

$$\begin{aligned} -\Lambda^2 &= \frac{2P_0}{\rho_1 a_1^2} - 2\pi G \rho_1 A_1 + \left(\frac{\partial^2 V_2}{\partial r^2} \right)_0 + \Omega^2 - 2\frac{a_2}{a_1} \Lambda \Omega, \\ -\Lambda^2 &= \frac{2P_0}{\rho_1 a_2^2} - 2\pi G \rho_1 A_2 + \frac{1}{R} \left(\frac{\partial V_2}{\partial r} \right)_0 + \Omega^2 - 2\frac{a_1}{a_2} \Lambda \Omega, \\ 0 &= \frac{2P_0}{\rho_1 a_3^2} - 2\pi G \rho_1 A_3 + \frac{1}{R} \left(\frac{\partial V_2}{\partial r} \right)_0. \end{aligned} \quad (5-14)$$

If we take the Newtonian potential as an interaction potential, Eq. (5·14) reduces to Eq. (2·15). Combining these equations with the angular velocity equation

$$\Omega^2 = -\frac{1+p}{R} \left(\frac{\partial V_2}{\partial r} \right)_0 (1+\delta), \quad (5-15)$$

where $p \equiv m_1/m_2$, we can construct equilibrium sequences.

5.3. Modified pseudo-Newtonian potential

Although there are a wide variety of choices of $V_2(r)$ to incorporate GR effects phenomenologically, we use the so called pseudo-Newtonian potential modifying the original form proposed by Paczyński and Wiita.³³⁾ This potential fits the effective potential for test particles orbiting Schwarzschild black hole quite well, as we will show later. We will use the modified pseudo-Newtonian potential defined by

$$V_2(r) = \frac{Gm_2}{r - r_{\text{pseudo}}}, \quad (5.16)$$

$$r_{\text{pseudo}} = r_s \{1 + g(p)\}, \quad (5.17)$$

$$g(p) = \frac{7.49p}{6(1+p)^2} - \frac{10.4p^2}{3(1+p)^4} + \frac{29.3p^3}{6(1+p)^6}, \quad (5.18)$$

$$r_s \equiv \frac{2GM_{\text{tot}}}{c^2}, \quad (5.19)$$

$$M_{\text{tot}} = m_1 + m_2, \quad (5.20)$$

where $g(p)$ is a correction term to fit the ISCOs obtained from the hybrid 2PN EOM of Kidder, Will, and Wiseman³²⁾. For $p = 0$, the modified pseudo-Newtonian potential agrees with the original pseudo-Newtonian potential proposed by Paczyński and Wiita.

Figure 11(a) shows effective potentials (solid lines) and locations of circular orbits (dots) in the modified pseudo-Newtonian potential ($p = 0$ and $r_{\text{pseudo}} = r_s$) and in the Schwarzschild metric. Although by this choice of the parameter ($r_{\text{pseudo}} = r_s$), the locations of the ISCOs in the modified pseudo-Newtonian potential agree with those in the Schwarzschild metric, the angular momenta at the ISCO are different, that is, the angular momentum in the modified pseudo-Newtonian potential (J_{pseudo}) for $p = 0$ is $(9/8)^{1/2}$ times larger than that in the Schwarzschild metric (J_{Sch}) at the ISCO. Therefore in Figs.11(a) and (b) we compare circular orbits with different angular momenta related as

$$J_{\text{pseudo}} = \left(\frac{9}{8}\right)^{1/2} J_{\text{Sch}}. \quad (5.21)$$

From Fig.11(b) we see that the radii of circular orbits of the modified pseudo-Newtonian potential agree with those of the effective potential around Schwarzschild black hole within 10% accuracy near the ISCO. This is the reason we believe that the modified pseudo-Newtonian potential defined here expresses the effect of general relativity within 10% accuracy so.

In the pseudo-Newtonian case, the quadrupole term δ is written as

$$\delta = \frac{3}{10} \left[2a_1^2 - \frac{(3R - r_{\text{pseudo}})(R - r_{\text{pseudo}})}{3R^2} (a_2^2 + a_3^2) \right] \frac{1}{(R - r_{\text{pseudo}})^2}. \quad (5.22)$$

When we take the limit $r_{\text{pseudo}} \rightarrow 0$, Eq. (5.22) recovers the Newtonian potential case (Eq. (5.7)).

5.4. The energy and the angular momentum

In this subsection, we show the total energy and angular momentum. We regard the minimum point of the total energy or the total angular momentum as the location of the ISCO.

The total energy is formally written as

$$E = T + W + W_i, \quad (5.23)$$

where T , W and W_i denote the kinetic, the self-gravity and the interaction energy, respectively. In the pseudo-Newtonian potential approach, T and W have the same form as that in the “pure” Newtonian case, but the interaction energy has the different form as

$$W_i = -\frac{Gm_1m_2}{R - r_{\text{pseudo}}} - \frac{Gm_2}{2(R - r_{\text{pseudo}})^3} \left[2I_{11} - \left(\frac{R - r_{\text{pseudo}}}{R} \right) (I_{22} + I_{33}) \right]. \quad (5.24)$$

Thus, the total energy is

$$E = \frac{m_1}{10} \left[\left(\Omega - \frac{a_2}{a_1} \Lambda \right)^2 a_1^2 + \left(\Omega - \frac{a_1}{a_2} \Lambda \right)^2 a_2^2 \right] + \frac{m_1 R^2}{2(1+p)} \Omega^2 - \frac{2}{5} \pi G \rho_1 m_1 A_0 - \frac{Gm_1m_2}{R - r_{\text{pseudo}}} - \frac{Gm_2}{2(R - r_{\text{pseudo}})^3} \left[2I_{11} - \left(\frac{R - r_{\text{pseudo}}}{R} \right) (I_{22} + I_{33}) \right], \quad (5.25)$$

where the angular velocity is written as

$$\Omega^2 = \frac{G(m_1 + m_2)}{R(R - r_{\text{pseudo}})^2} \left[1 + \frac{3}{10(R - r_{\text{pseudo}})^2} \left\{ 2a_1^2 - \frac{(3R - r_{\text{pseudo}})(R - r_{\text{pseudo}})}{3R^2} (a_2^2 + a_3^2) \right\} \right]. \quad (5.26)$$

The form of the total angular momentum in the pseudo-Newtonian potential approach is the same as that in the pure Newtonian case as

$$J = \frac{m_1 R^2}{1+p} \Omega + \frac{m_1}{5} (a_1^2 + a_2^2) \Omega - \frac{2}{5} m_1 a_1 a_2 \Lambda. \quad (5.27)$$

Note that the pseudo-Newtonian effect is included implicitly in the angular velocity.

5.5. Results

In previous subsections, we described equations needed to get equilibrium sequences and to determine the location of the ISCO. Here, we show the results for the equal mass binary ($p = 1$) in the corotating case ($f_R = 0$) and the irrotational case ($f_R = -2$).

In Figs.12 and 13, we show $\tilde{E}(a)$ and $\tilde{J}(b)$ as functions of $\tilde{\Omega}$ in the corotating and irrotational cases, respectively. Note that the minima for the energy and angular

momentum denote the ISCCO for $f_R = 0$ case, and the ISCO for $f_R = -2$ case. In Fig.14, we show $\bar{\Omega} \equiv \Omega(Gm_1/c^3)$ at the ISCO and/or ISCCO as a function of the compactness parameter of star 1 Gm_1/a_0c^2 for $p = 1$. Note that this normalization is different from that in Fig.7 and so on. In this normalization, the orbital angular velocity of the Newtonian order (the value at $Gm_1/a_0c^2 = 0$) becomes zero, and it is not convenient to compare $\bar{\Omega}$ with the Newtonian angular velocity. However, the approach of TN is based on the point particle binary case, i.e., the case of $Gm_1/a_0c^2 \rightarrow \infty$. Then, it is natural to choose the normalization $\bar{\Omega}$ in this section.

From these figures, we find that due to the finite size effect of the star, $\bar{\Omega}$ at the ISCO (ISCCO) is always smaller than the point particle limit ($\bar{\Omega}=0.0402$) i.e. the finite size effect of the star always destabilize the binary. However as a function of the relativity parameter, $\bar{\Omega}$ at the ISCO (ISCCO) increases which is qualitatively the same result as in 1PN treatment. In this sense there is no disagreement between 1PN and the result in this section apparently.

5.6. 1PN calculations without 1PN self-gravity effect

One of the unsatisfactory points in TN is that the PN effect of the self-gravity is not included. While in 1PN calculations in §3 and §4, 1PN effect of the self-gravity as well as the gravity between two stars are consistently taken into account. In §4 we suggested that 1PN effect of the self-gravity will have stabilizing effect. To expect PN effect of the self-gravity in TN in this subsection we will calculate $\bar{\Omega}$ at the ISCCO removing the 1PN self-gravity terms in the calculations of §3.

5.6.1. Equations

As mentioned above, we only incorporate the PN effect only to the gravity acting between two stars in this approximation. So that equations we use are quite similar to those in §2.1 except for the angular velocity which we use

$$\Omega^2 = \frac{2GM}{R^3} \left[1 + \frac{3}{5R^2}(2a_1^2 - a_2^2 - a_3^2) \right] - \frac{9G^2M^2}{2R^4c^2}. \quad (5.28)$$

Here the PN effect appears in the last term. (Note that for $a_1, a_2, a_3 \rightarrow 0$, the angular velocity agrees with that for two point masses.) As in §2.1, we use Eqs. (2.15) to determine $\alpha_2 = a_2/a_1$ and $\alpha_3 = a_3/a_1$.

In calculating equilibrium sequences, we must fix the conserved mass M_* (see Eq. (3.42)). In this section, the conserved mass should be written as

$$M_* = M \left(1 + \frac{13GM}{4Rc^2} \right), \quad (5.29)$$

where we neglect the stellar structure terms in the 1PN order.

As was done in previous sections, we regard the minimum of the energy as the location of the ISCO. In this approximation, the energy is written as

$$E = -\frac{3GM^2}{5a_0^3}A_0 - \frac{GM^2}{2R} + \frac{GM^2}{10R^3}(2a_1^2 - a_2^2 - a_3^2)$$

$$\begin{aligned}
& + \frac{M}{5} \Omega_{\text{N}}^2 \left[(a_1^2 + a_2^2) \left\{ 1 + \left(\frac{a_1 a_2 f_R}{a_1^2 + a_2^2} \right)^2 \right\} + \frac{4a_1^2 a_2^2}{a_1^2 + a_2^2} f_R \right] \\
& - \frac{25G^2 M^3}{16R^2 c^2}, \tag{5-30}
\end{aligned}$$

where a_0 denotes the radius of the spherical star in the Newtonian order.

5.6.2. Results

In the following calculation, we normalize the angular velocity and the energy by $(GM_*/a_*^3)^{1/2}$ and GM_*^2/a_* , respectively, where a_* represents the radius of the PN spherical star defined by the conserved mass as

$$a_* \equiv \left(\frac{3M_*}{4\pi\rho} \right)^{1/3} = a_0 \left(1 + \frac{13GM_*}{12Rc^2} \right). \tag{5-31}$$

The normalized angular velocity and energy are written as

$$\begin{aligned}
\tilde{\Omega}^2 &= \frac{2\alpha_2\alpha_3}{\tilde{R}^3} \left[1 + \frac{3}{5\tilde{R}^2} (2 - \alpha_2^2 - \alpha_3^2) \right] - \frac{9(\alpha_2\alpha_3)^{4/3}}{2\tilde{R}^4} C_s, \tag{5-32} \\
\tilde{E} &= (\alpha_2\alpha_3)^{1/3} \left[-\frac{3}{5} \frac{\tilde{A}_0}{\alpha_2\alpha_3} - \frac{1}{2\tilde{R}} + \frac{1}{10\tilde{R}^3} (2 - \alpha_2^2 - \alpha_3^2) \right. \\
&\quad \left. + \frac{\tilde{\Omega}_{\text{N}}^2}{5\alpha_2\alpha_3} \left\{ (1 + \alpha_2^2) \left\{ 1 + \left(\frac{\alpha_2 f_R}{1 + \alpha_2^2} \right)^2 \right\} + \frac{4\alpha_2^2}{1 + \alpha_2^2} f_R \right\} \right] \\
&\quad + \frac{55(\alpha_2\alpha_3)^{2/3}}{48\tilde{R}^2} C_s, \tag{5-33}
\end{aligned}$$

where $\tilde{R} = R/a_1$ and $C_s \equiv GM_*/c^2 a_*$.

Figures 15(a) and (b) show the energy as a function of the angular velocity in the corotating case ($f_R = 0$) and the irrotational one ($f_R = -2$), respectively. The solid, dotted, short dashed, and long dashed lines represent the cases for $C_s = 0, 0.01, 0.03$ and 0.05 , respectively. Note that for $f_R = -2$, the minima correspond to the ISCO and for $f_R = 0$, the minima correspond to the ISCCO. In Fig.16, we show $\tilde{\Omega}$ at the ISCCO as a function of C_s with (the dotted line) or without (the solid line) 1PN effect of the self-gravity, where we use the normalization $\tilde{\Omega}$ to present Fig.16 in order to compare it with Fig.14. As expected the dotted line is above the solid line. Therefore from these calculations we can say that the 1PN effect of the self-gravity will increase $\tilde{\Omega}$ and stabilize the binary. Note here that the Fig.16 corresponds to the lower left corner of Fig.14. We checked the numerical value of $\tilde{\Omega}$ in the solid lines of Fig.14 and Fig.16 for the same relativity parameter and found the almost similar value. This is not strange. For small relativity parameter both treatments essentially agree since the pseudo-Newtonian potential is almost the same as the Newtonian potential. Therefore this result suggests that at least for small relativity parameter if we include 1PN effect of the self-gravity to TN, $\tilde{\Omega}$ at ISCO (ISCCO) will increase. What will happen for large relativity parameter is not certain but we expect that the tendency will not change.

§6. Brief review on recent semi-relativistic works

So far, we have investigated the location of the ISCO in the PN approximation. Although we have obtained qualitative properties of the GR correction for the location of the ISCO, the PN study is not sufficient to know the location accurately because it is accurate for small C_s , but NS is a highly GR star of $C_s \sim 0.2$. Thus, we need calculation including full GR terms or sufficient GR corrections. In the fully GR case, there is no equilibrium state of BNSs because of emission of GWs. Even so, we will be able to consider quasi-equilibrium states because t_{GW} is still much longer than the orbital period for orbits outside the ISCO. However, we have not known yet how to define the “quasi-equilibrium” in the fully GR case in contrast to the 1PN and 2PN cases in which we can distinguish quantities related to GWs from others. Thus, for fully GR calculation, we must begin from the unresolved first step, where we need to clarify the notion of the “quasi-equilibrium” and establish the formulation along the notion.

Instead of fully GR one, two groups have been performing semi-GR calculation.^{34) 35)} The essence of their method is to assume that the three metric has the conformal flat form approximately. In this case, all the geometric variables which appear in the formalism are determined by solving Poisson equations, and wave equations do not appear. Thus, effect of GWs is neglected and the formalism reduces to that similar to the PN one. Although some fully GR effects are taken into account in this formalism, the meaning of this approximation is still not sure. For example, if the orbital separation of BNSs is sufficiently large (i.e., tidal effects are not important) and spin angular velocity of each star is negligible, this formalism yields the exact GR solution. On the other hand, from the PN point of view, the formalism includes all the 1PN terms consistently, but not the 2PN terms when close BNSs are concerned. Thus, we may regard it as a formalism in which some GR corrections are merely included in the 1PN approximation.

For a small compactness C_s , this formalism will yield the same answer as that obtained by the 1PN calculation. Actually, this is the case for numerical results by Baumgarte et al. (BCSST):³⁵⁾ They obtained equilibrium states of corotating BNSs and their numerical results agree with those obtained in §4 for small C_s cases, and even for large C_s , they are similar to ours. From this fact, we may consider that this formalism is essentially very similar to the 1PN one. On the other hand, Wilson et al. did not obtain equilibrium states of corotating binary, but of non-uniform internal motion. Since the velocity field is different from the uniformly rotating one, the results may quantitatively disagree with ours and BCSST. However, qualitative nature also does not at all agree with ours and BCSST; in the analysis by Wilson et al., (1) Ω_{ISCO} decreases with increase of the GR effect and (2) the maximum density increases with decrease of the orbital separation, while the opposite relation holds in the analysis of ours and BCSST. There have been several researchers who doubt that accuracy of their calculation is not enough and their results are something incorrect.^{36) 35) 13)} However, we cannot completely deny a possibility that we miss some GR effects we have not been aware of. We may not reach a certain conclusion even for the case of this simplest version of semi-GR calculation at present. Hence,

to clarify the meaning of this approximation and accuracy of their numerical results, many works should be done in this area in near future.

§7. Summary

In this manuscript, we have presented recent results obtained from the study on the location of the ISCO in several levels of the PN approximation. The following is the brief summary.

- Even in the Newtonian case, there exists the ISCO for binary of sufficiently stiff EOS. If the mass and the radius of each star are fixed, Ω_{ISCO} is larger for softer EOS.
- There exist roughly two kinds of the 1PN corrections. One is the correction to the self-gravity of each star of binary, and the other is the correction to the gravity acting between two stars. The former one tends to increase Ω_{ISCO} , but the latter one tends to decrease it. If we take into account both effects, however, the former effect is stronger than the latter one, and Ω_{ISCO} becomes large with increase of the 1PN correction.
- The feature mentioned above is more remarkable for softer EOS when we fix the mass and radius. This is because for softer EOS, each star has the larger central density and is susceptible to the GR correction.
- There has been no self consistent calculation including all the 2PN effects. But, there exist studies in which one only considers the 2PN gravity acting between two stars. In this case, Ω_{ISCO} is always smaller than that for the Newtonian case. If we include the PN effect of the self-gravity, Ω_{ISCO} will increase.

Acknowledgment

Numerical computations were mainly performed on FACOM VX4 in data processing center of National Astronomical Observatory in Japan. This work was in part supported by a Grant-in-Aid for Science Research from the Ministry of Education, Culture, Science and Sports (08NP0801, 08237210 and 09740336).

References

- [1] A. Abramovici et al., *Science* **256** (1992), 325.
- [2] C. Bradaschia et al., *Nucl. Instrum. and Methods* **A289** (1990), 518.
- [3] J. Hough, in *Proceedings of the Sixth Marcel Grossmann Meeting*, edited by H. Sato and T. Nakamura (World Scientific, Singapore, 1992), p.192.
- [4] K. Kuroda et al. in *Proceedings of the international conference on gravitational waves: Sources and Detectors*, edited by I. Ciufolini and F. Fiducard (World Scientific, 1997), p.100.
- [5] K. S. Thorne, in *300 Years of Gravitation*, edited by S. Hawking and W. Israel (Cambridge University Press, 1987), p.330.
- [6] C. Cutler et al., *Phys. Rev. Lett.* **70** (1993), 2984.
- [7] X. Zunge, J. M. Centrella, and S. L. W. Mcmillan, *Phys. Rev. D* **50** (1994), 6247; **54** (1996), 7261.
- [8] L. Lindblom, *Astrophys. J.* **398** (1992), 569.
- [9] D. Lai, F. A. Rasio, and S. L. Shapiro, *Astrophys. J. Suppl.* **88** (1993), 205.
- [10] D. Lai, F. A. Rasio, and S. L. Shapiro, *Astrophys. J.* **420** (1994), 811.

- [11] M. Shibata, *Prog. Theor. Phys.* **96** (1996), 317; *Phys. Rev. D* **55** (1997), 6019.
- [12] K. Taniguchi and M. Shibata, *Phys. Rev. D* **56** (1997), 798.
- [13] M. Shibata and K. Taniguchi, *Phys. Rev. D* **56** (1997), 811.
- [14] K. Taniguchi and T. Nakamura(TN), *Prog. Theor. Phys.* **96** (1996), 693.
- [15] D. Lai and A. G. Wiseman(LW), *Phys. Rev. D* **54** (1996), 3958.
- [16] W. Ogawaguchi and Y. Kojima, *Prog. Theor. Phys.* **96** (1996), 901.
- [17] H. Goldstein, *Classical Mechanics* (Addison-Wesley, Reading, MA, 1980).
- [18] S. Chandrasekhar, *Ellipsoidal Figures of Equilibrium* (Yale University Press, NewHaven, 1969).
- [19] C. S. Kochanek, *Astrophys. J.* **398** (1992), 234.
L. Bildsten and C. Cutler, *Astrophys. J.* **400** (1992), 175.
- [20] E. Flowers and N. Itoh, *Astrophys. J.* **206**(1976), 218; **230** (1979), 847.
- [21] J. L. Friedman, J. R. Ipser and L. Parker, *Astrophys. J.* **304** (1986), 115.
G. B. Cook, S. L. Shapiro, and S. A. Teukolsky, *astrophys. J.* **398** (1992), 203; **424** (1994), 823.
- [22] For example, S. L. Shapiro and S. A. Teukolsky, *Black Holes, White Dwarfs, and Neutron Stars* (New York, Wiley, 1983).
- [23] For example, J. H. Taylor, R. N. Manchester, and G. Lyne, *Astrophys. J. Suppl.* **88**(1993), 529.
- [24] I. Hachisu, *Astrophys. J. Suppl.* **61** (1986), 479.
K. Oohara and T. Nakamura, *Prog. Theor. Phys.* **83** (1990), 906.
- [25] S. Chandrasekhar, *Astrophys. J.* **148** (1967), 621; and also see nice collection, *Selected Papers*, S. Chandrasekhar (Chicago University Press, 1990), Vol.5.
- [26] H. Asada and M. Shibata, *Phys. Rev. D* **54** (1996), 4944.
See also H. Asada and T. Futamase (this volume).
- [27] S. Chandrasekhar, *Astrophys. J.* **142** (1965), 1488.
- [28] C. M. Will, *Theory and Experiment in Gravitational Physics* (Cambridge University Press, Cambridge, 1981), p.146.
- [29] L. Blanchet, T. Damour, B. R. Iyer, C. M. Will, and A. G. Wiseman, *Phys. Rev. Lett.* **74** (1995), 3515.
L. Blanchet, T. Damour, and B. R. Iyer, *Phys. Rev. D* **51** (1995), 5360.
C. M. Will and A. G. Wiseman, *ibid.* **54** (1996), 4813.
- [30] L. E. Kidder, C. M. Will, and A. G. Wiseman, *Phys. Rev. D* **47** (1993), R4183.
L. E. Kidder, *Phys. Rev. D* **52** (1995), 821.
- [31] J. C. Lombardi, Jr., F. A. Rasio, and S. L. Shapiro, *Phys. Rev. D* **56** (1997), 3416.
- [32] L. E. Kidder, C. M. Will, and A. G. Wiseman, *Phys. Rev. D* **47** (1993), 3281.
- [33] B. Paczyński and P. J. Wiita, *Astron. Astrophys.* **88** (1980), 23.
- [34] J. R. Wilson, G. J. Mathews and P. Marronetti, *Phys. Rev. D* **54** (1996), 1317.
- [35] T. W. Baumgarte, S. L. Shapiro, G. B. Cook, M. A. Scheel, and S. A. Teukolsky, Preprint gr-qc/9701033; *Phys. Rev. Lett.* **79** (1997), 1182; Preprint gr-qc/9709026.
- [36] D. Lai, *Phys. Rev. Lett.* **76** (1996), 4878.
P. R. Brady and S. A. Hughes, *Phys. Rev. Lett.* **79** (1997), 1186.
A. G. Wiseman, *Phys. Rev. Lett.* **79** (1997), 1189.
E. E. Flanagan, Preprint gr-qc/9706045:
K. S. Thorne, *Phys. Rev. D*(to be published), Preprint gr-qc/9706057.

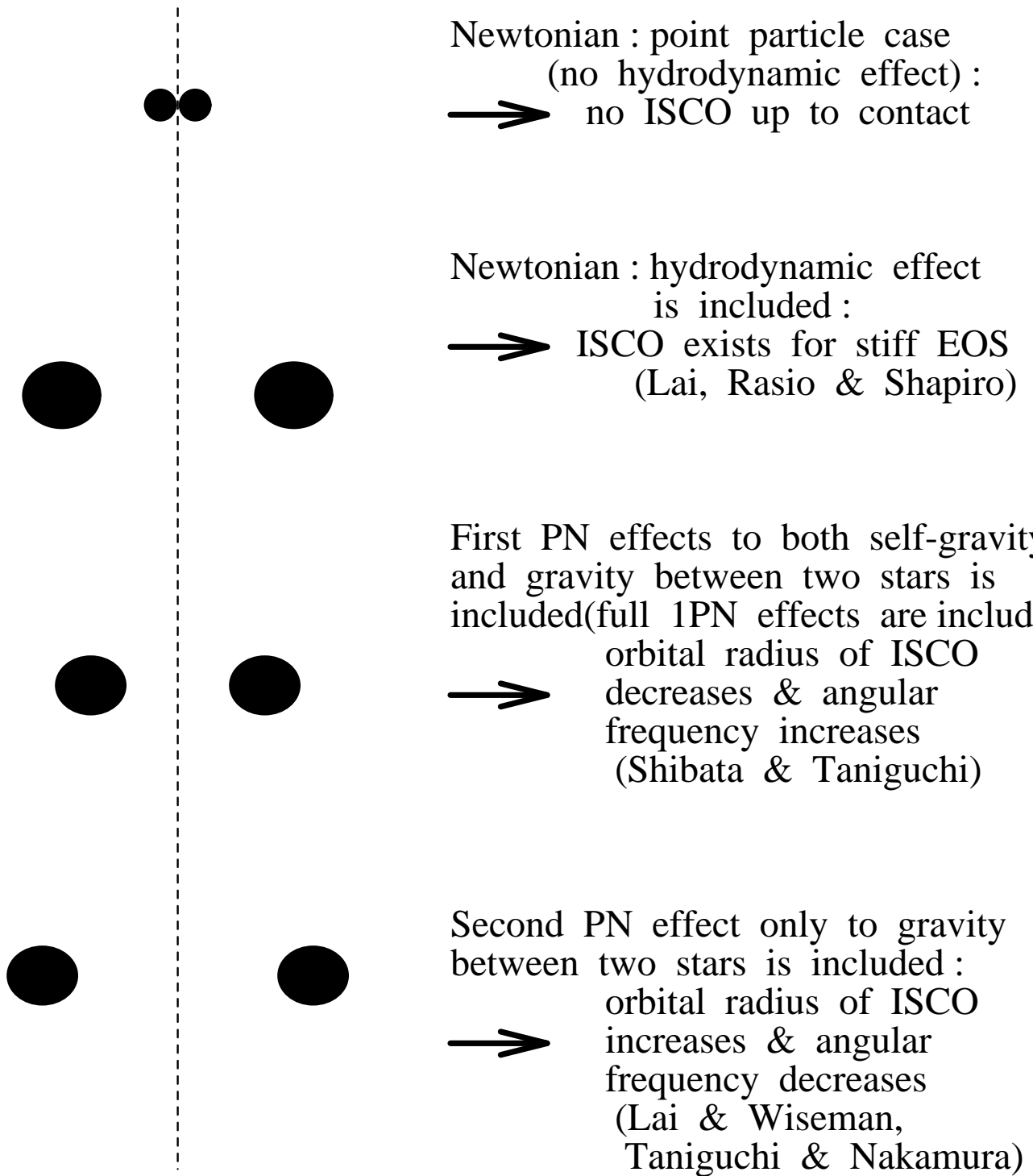
FIGURE CAPTIONS

- Fig.1: Location of the ISCO is shown in each level of approximation, schematically.
- Fig.2: Sketch of corotating binary. The origin of the coordinate is located at the center of mass of star 1.
- Fig.3: The energy(a) and the angular momentum(b) as functions of the angular velocity for Newtonian incompressible binary stars of $C/(GMa_0)^{1/2} = -2, -1.5, -1, -0.5, 0, 0.5, 1, 1.5, 2$ and corotating binary.

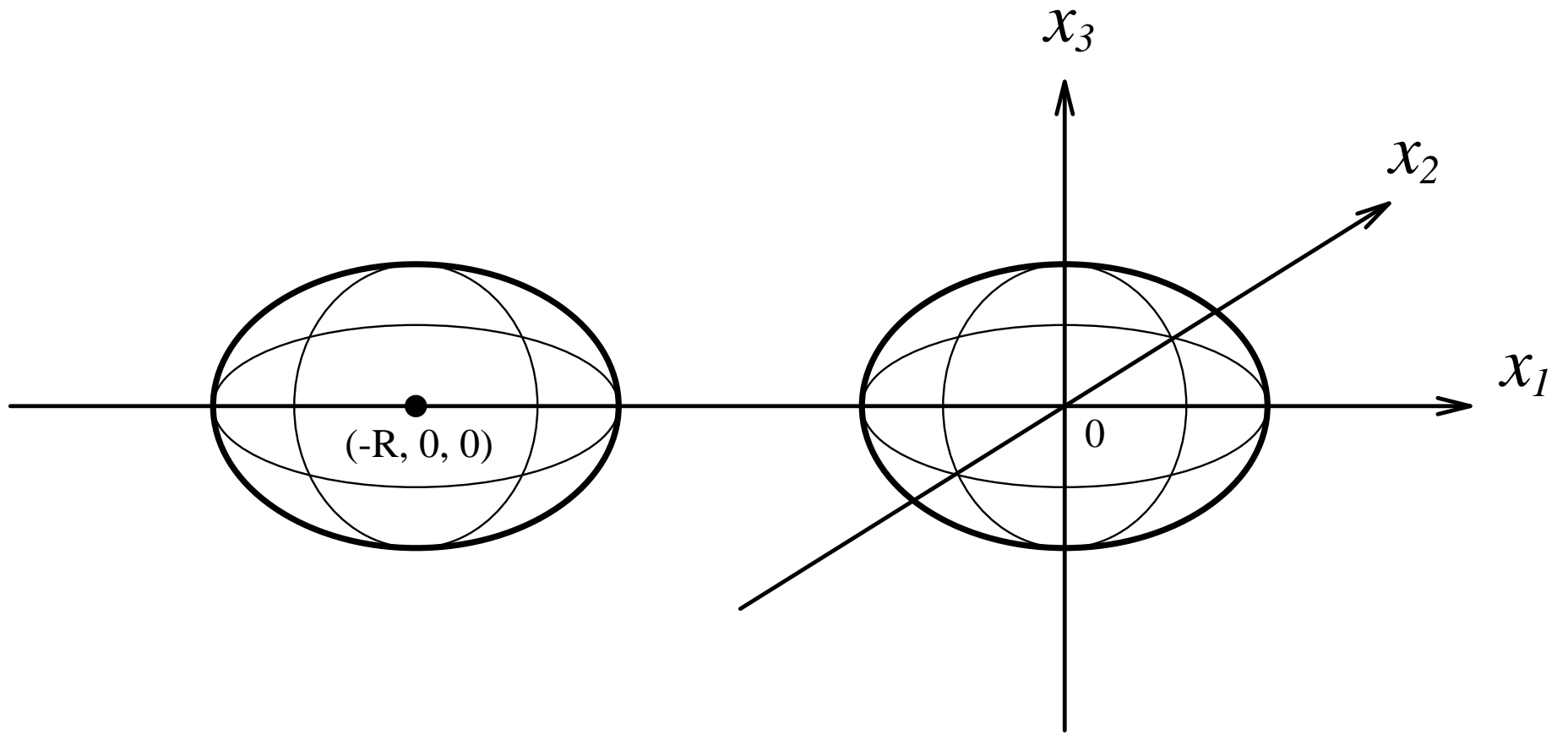
- Fig.4: The energy and the angular momentum as functions of the angular velocity for Newtonian corotating binary of compressible EOS. (a) for $n = 0.25$, (b) for $n = 0.5$, (c) for $n = 0.75$ and (d) for $n = 1$.
- Fig.5: $\Omega_{\text{N:ISCCO}}/\Omega_0$ as a function of the polytropic index n . Solid line denotes $0.248(1+0.2n^{1.5})$. Note that $\Omega_{\text{N:ISCCO}}$ was determined with $\sim \pm 1\%$ uncertainty.
- Fig.6: The total energy(a) and angular momentum(b) of the equilibrium sequence as functions of Ω/Ω_* for 1PN incompressible binary stars. Solid, dotted, dashed and long dashed lines denote $C_s = GM_*/c^2 a_* = 0$ (the Newtonian case), 0.01, 0.03 and 0.05, respectively.
- Fig.7: The orbital angular velocity at the ISCCO as a function of the compactness parameter $C_s \equiv GM_*/c^2 a_*$ for 1PN incompressible binary stars.
- Fig.8: The relation between R_*/a_* and Ω/Ω_* for $n = 0.5$ and $C_s = 0$ (open circles), 0.0327 (filled circles) and 0.0654 (filled squares). Dotted lines are drawn using Eq. (4.5) as counter parts of numerical results.
- Fig.9: The energy and angular momentum as functions of Ω/Ω_* for $n = 0.5$ (a), 0.75(b) and 1(c) for the 1PN case. In Fig.9(a), open circles, filled circles and open squares denotes sequences for $C_s = 0, 0.0327$ and 0.0654 , in Fig.9(b), they denote sequences for $C_s = 0, 0.02$ and 0.04 , and in Fig.9(c), they denote sequences for $C_s = 0, 0.0167$ and 0.0333 , respectively.
- Fig.10: The angular velocity at the ISCCO as a function of C_s for $n = 0.5$ (a), 0.75(b) and 1(c). Note that Ω_{ISCCO} was determined with $\sim \pm 1\%$ uncertainty.
- Fig.11: (a)The effective potentials of a test particle in the Schwarzschild metric (left) and the pseudo-Newtonian potential (right) as a function of the normalized distance R/r_s . The vertical axes denote $\Psi_{\text{Sch}} = \sqrt{(1 - (2GM/Rc^2))((G^2 J_{\text{Sch}}^2/R^2 c^6) + 1)} - 1$ and $\Psi_{\text{pseudo}} = -(GM/(R - r_s)c^2) + (G^2 J_{\text{pseudo}}^2/2R^2 c^6)$, respectively. The dots express the place of circular orbits. The value of the effective potential of the Schwarzschild black hole at the infinity is shifted to zero. (b)The fractional deviation of circular orbits of the pseudo-Newtonian potential from those of the Schwarzschild effective potential as a function of of the angular momentum. Circular orbits with different angular momentum related as $J_{\text{pseudo}} = (9/8)^{1/2} J_{\text{Sch}}$ are compared (see text).
- Fig.12: The total energy(a) and angular momentum(b) of the equilibrium sequences as functions of the angular velocity in the case of corotating binaries. Solid, dotted, short dashed, long dashed, short dash-dotted, and long dash-dotted lines denote $Gm_1/a_0c^2 = 0.05, 0.1, 0.15, 0.2$ and 0.25 , respectively.
- Fig.13: The total energy(a) and angular momentum(b) for irrotational binaries as functions of the angular velocity. The conventions are the same as in Fig.12.
- Fig.14: The relation between the compactness of star 1 (Gm_1/a_0c^2) and the angular velocity of the binary $\tilde{\Omega} = \Omega(Gm_1/c^3)$ at the ISCO. Solid and dashed lines denote the cases of the corotating (Roche Ellipsoids) and irrotational binaries (Irrotational Roche-Riemann Ellipsoids), respectively. The value written at the upper right corner is that of the angular velocity in the point particle binary case.

- Fig.15: The 1PN total energy without self-gravity terms as a function of the angular velocity in the corotating case(a) and the irrotational one(b), respectively. Solid, dotted, short dashed and long dashed lines represent the cases for $C_s = 0, 0.01, 0.03$ and 0.05 , respectively.
- Fig.16: The relation between C_s and $\bar{\Omega} = \Omega(GM_*/c^3)$ at the ISCCO. Solid and dotted lines denote the cases of the 1PN corotating binaries without and with the 1PN self-gravity, respectively.

Location of the ISCO in several levels of PN approximation

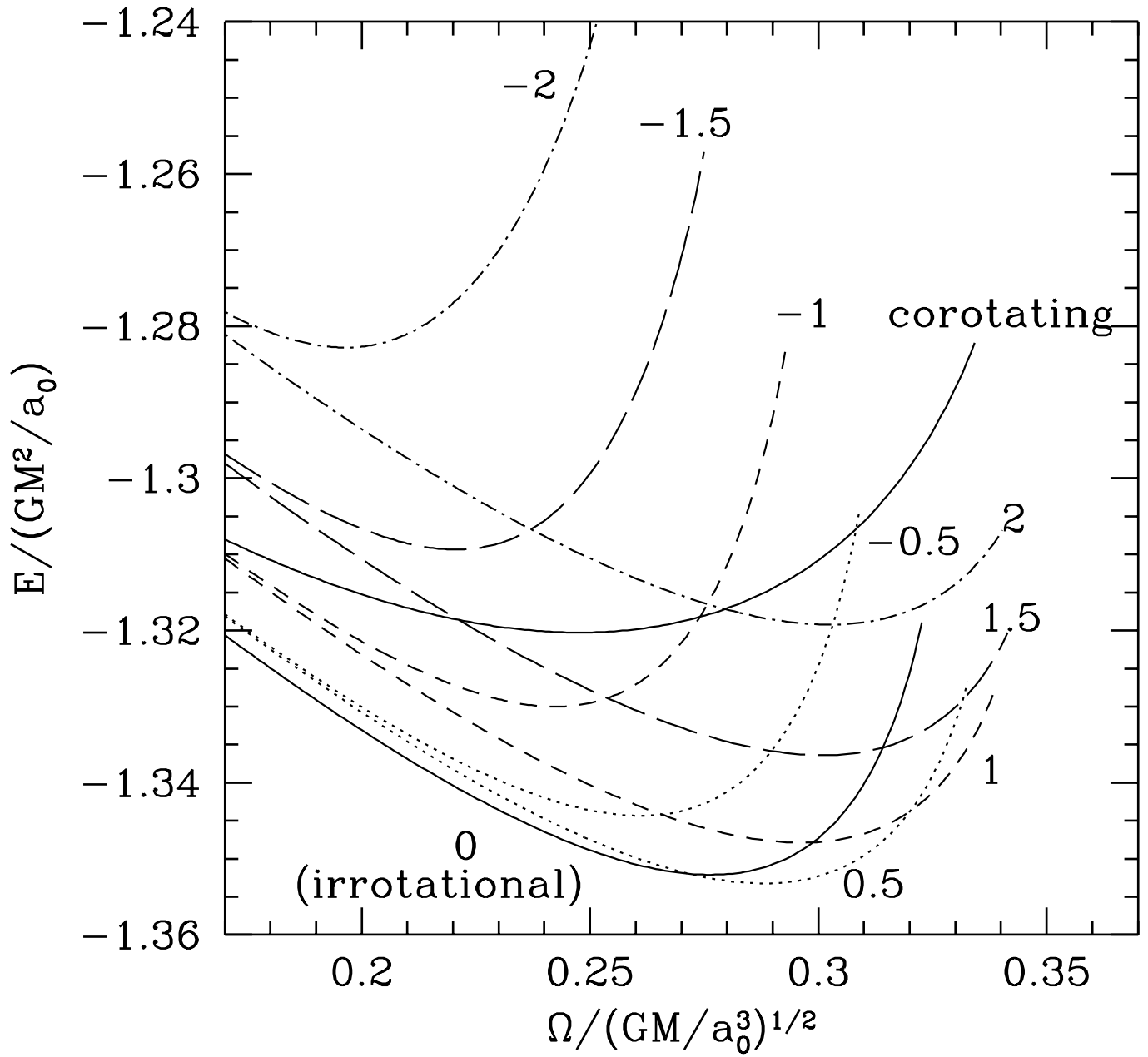


Full 2PN, Full GR : not yet performed

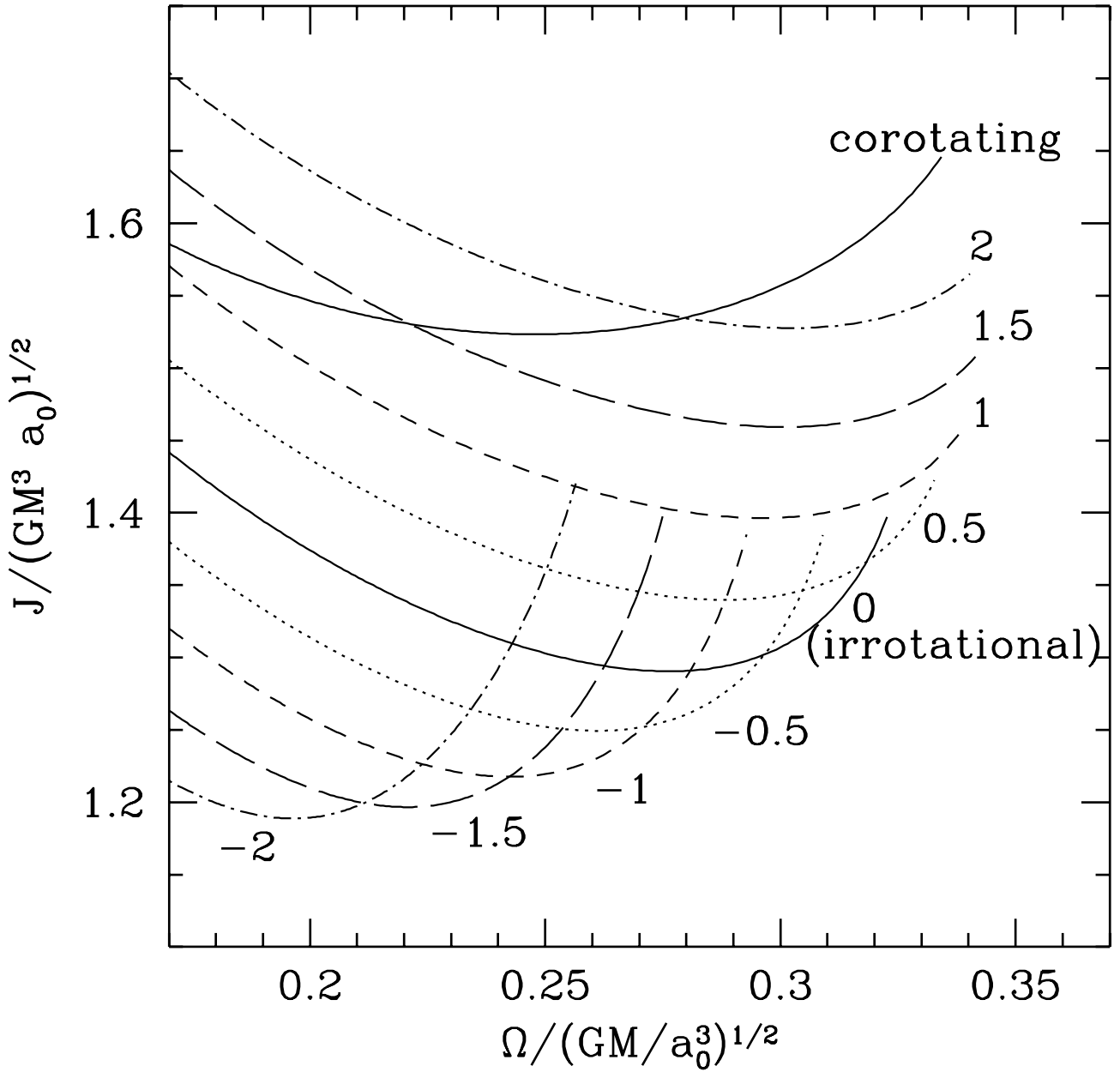


Star 2

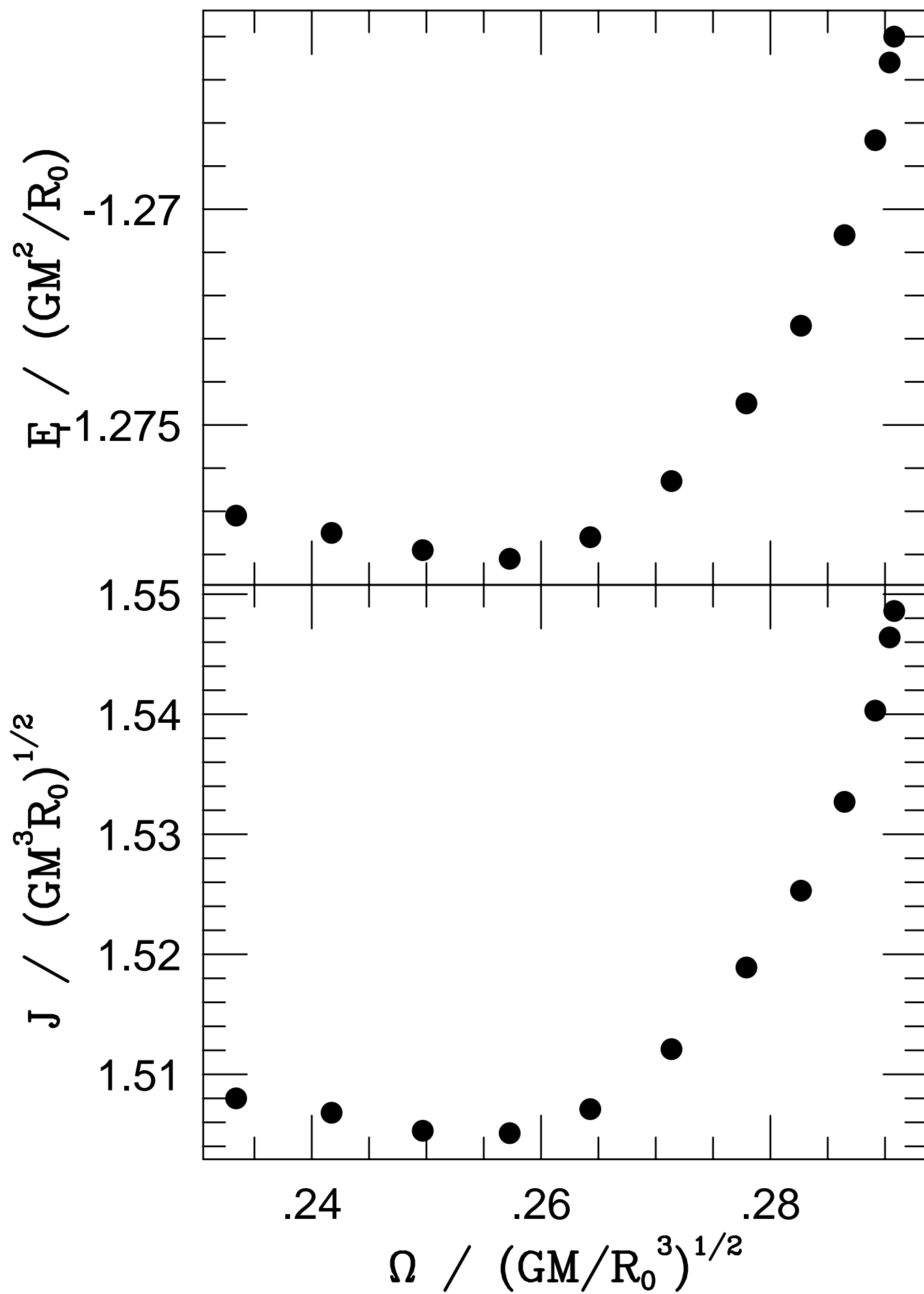
Star 1

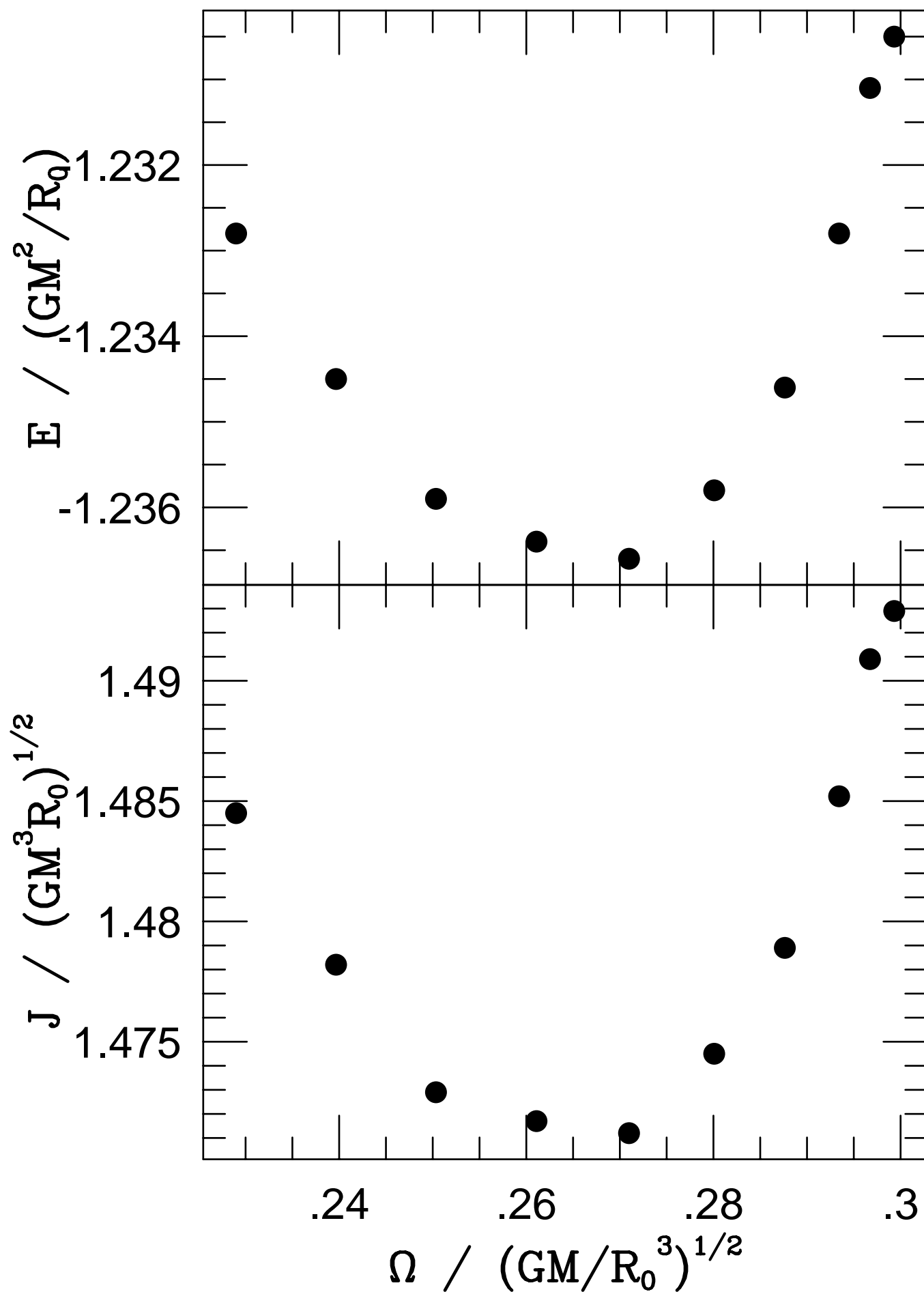


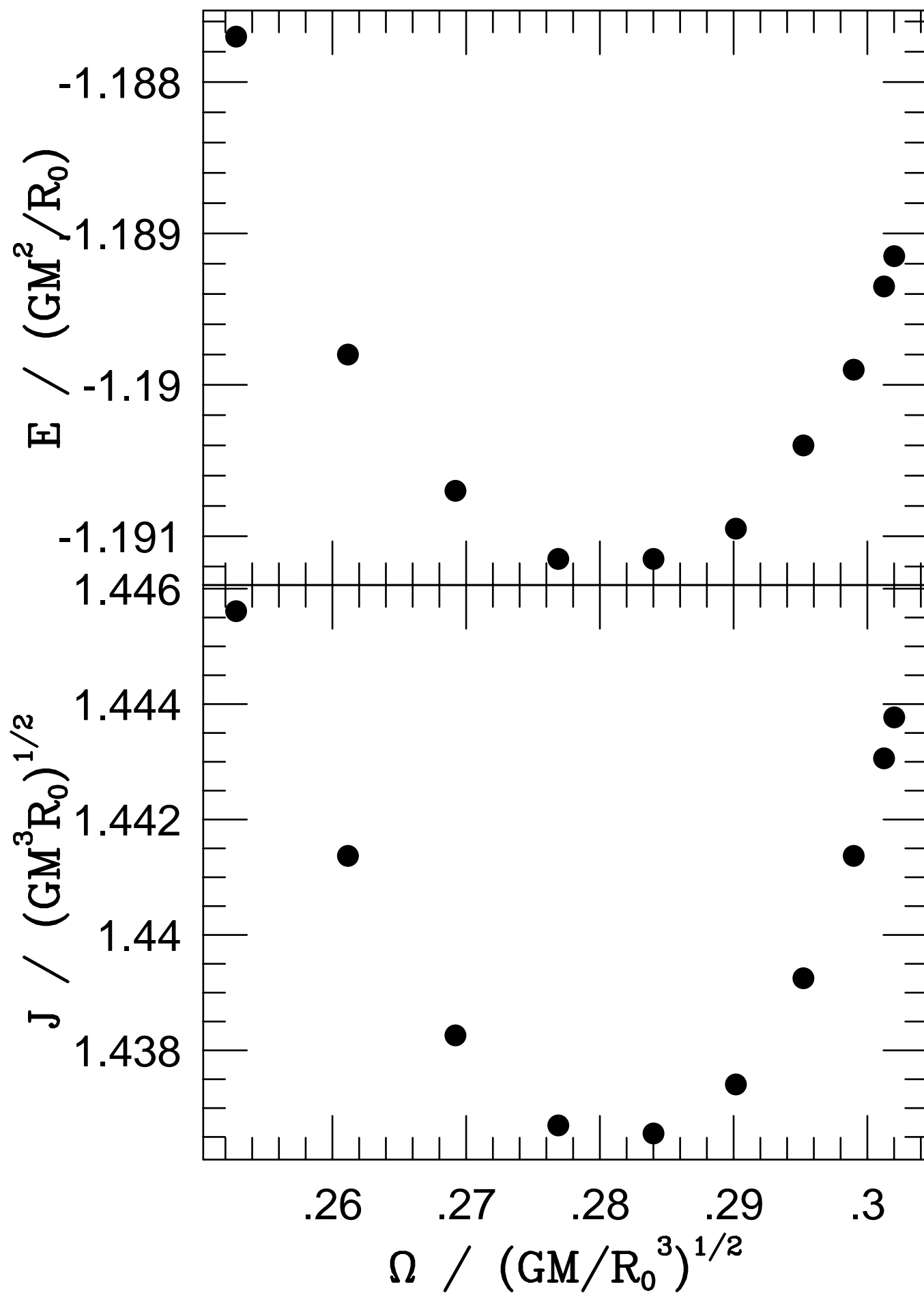
(a)

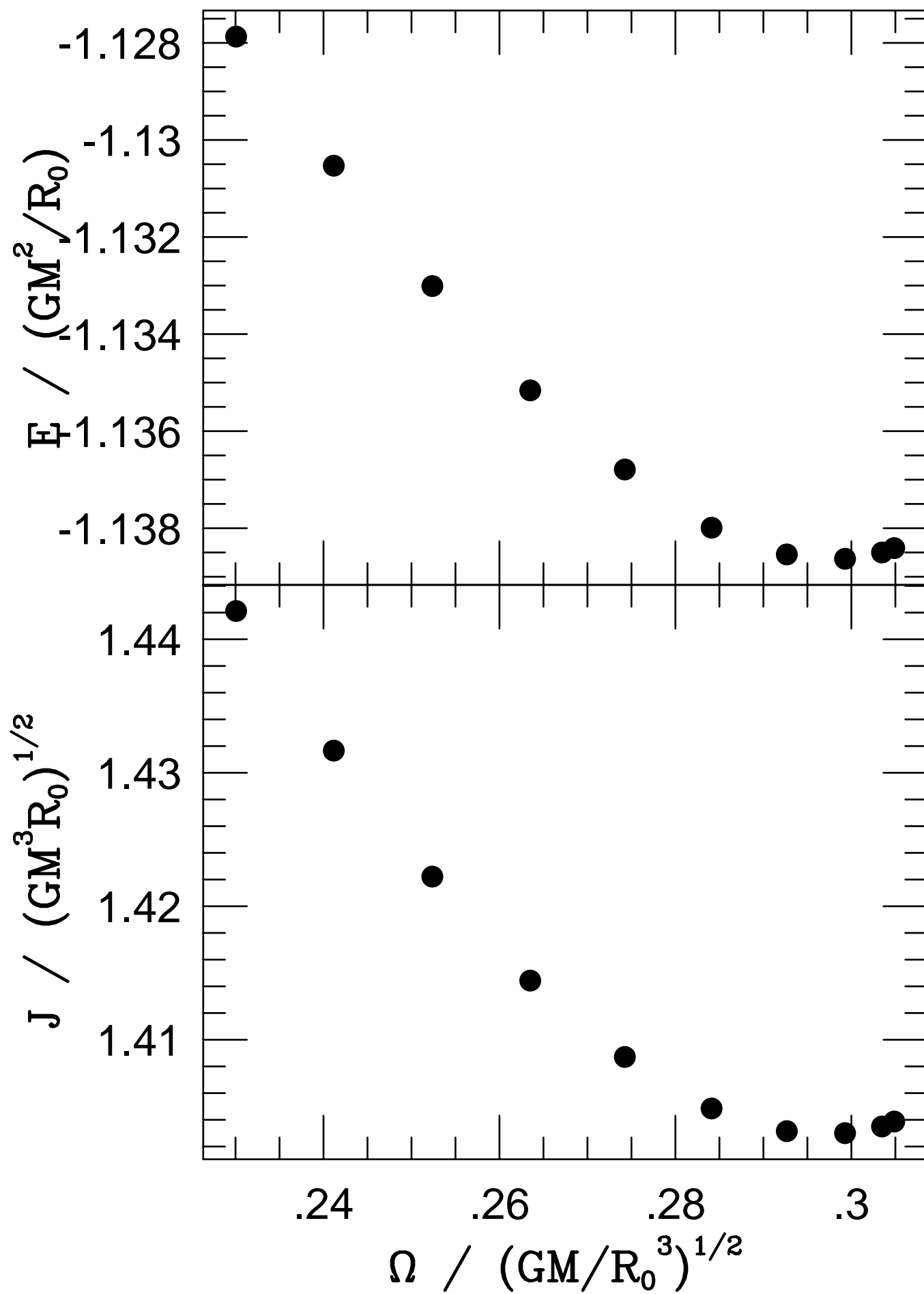


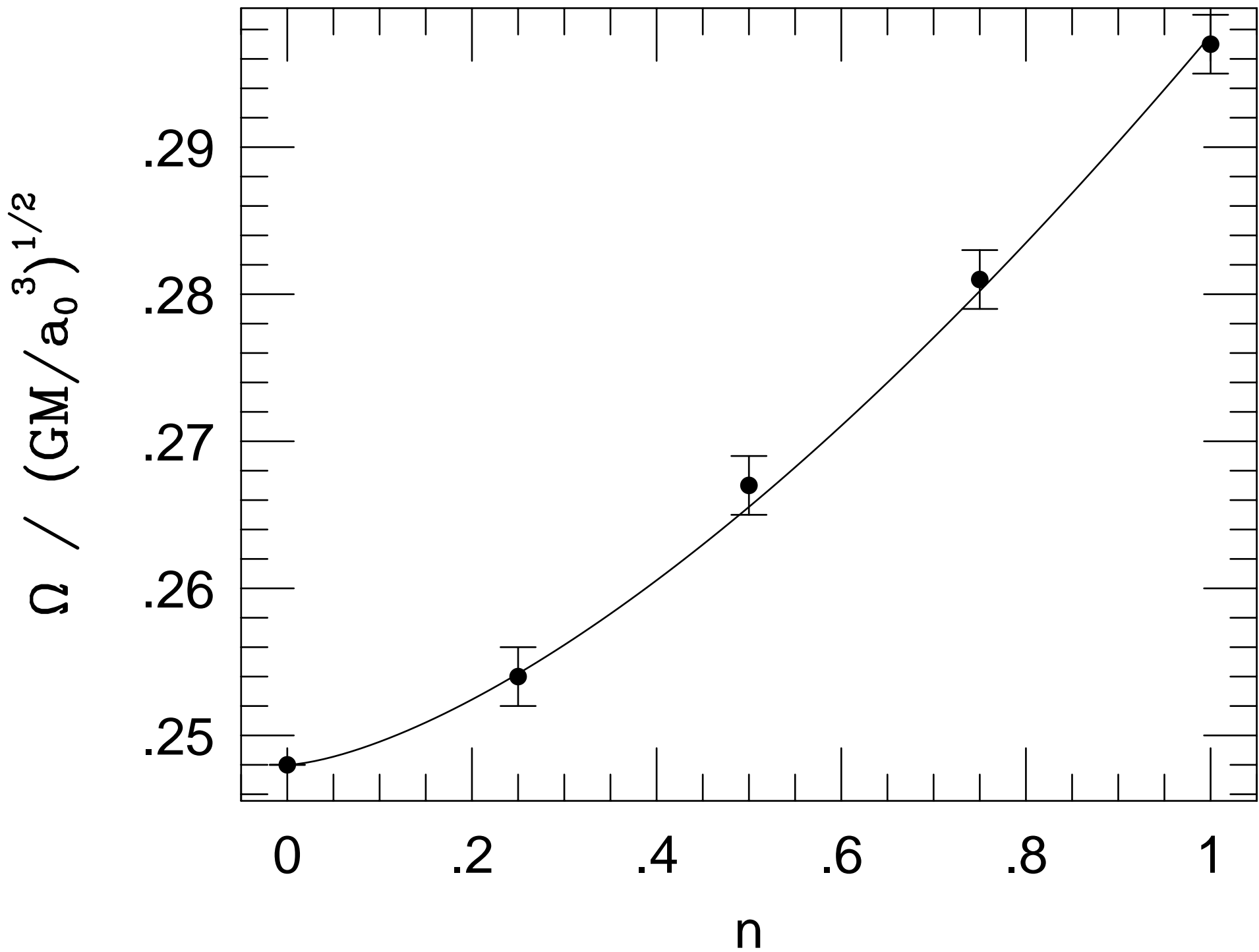
(b)

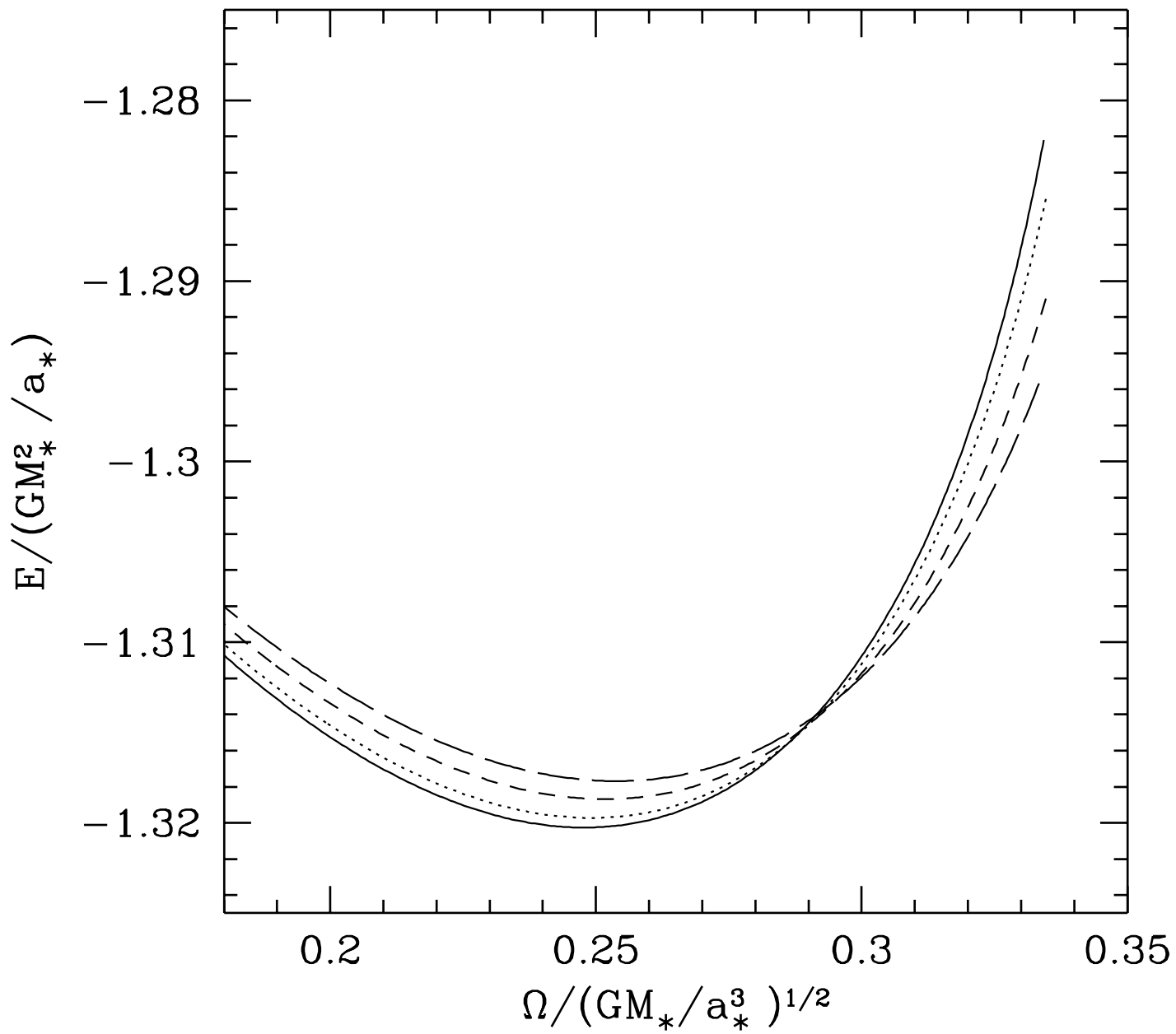




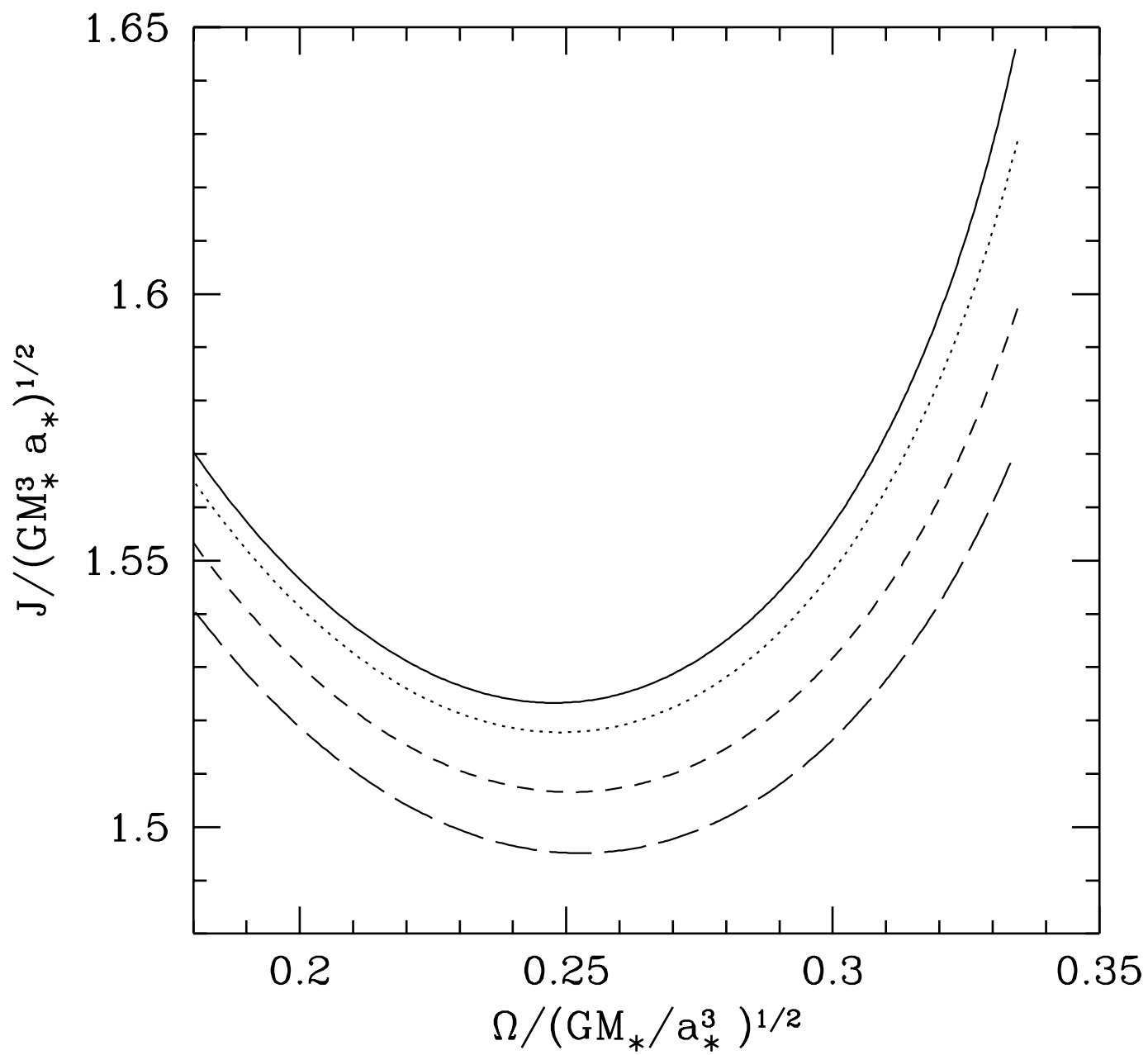




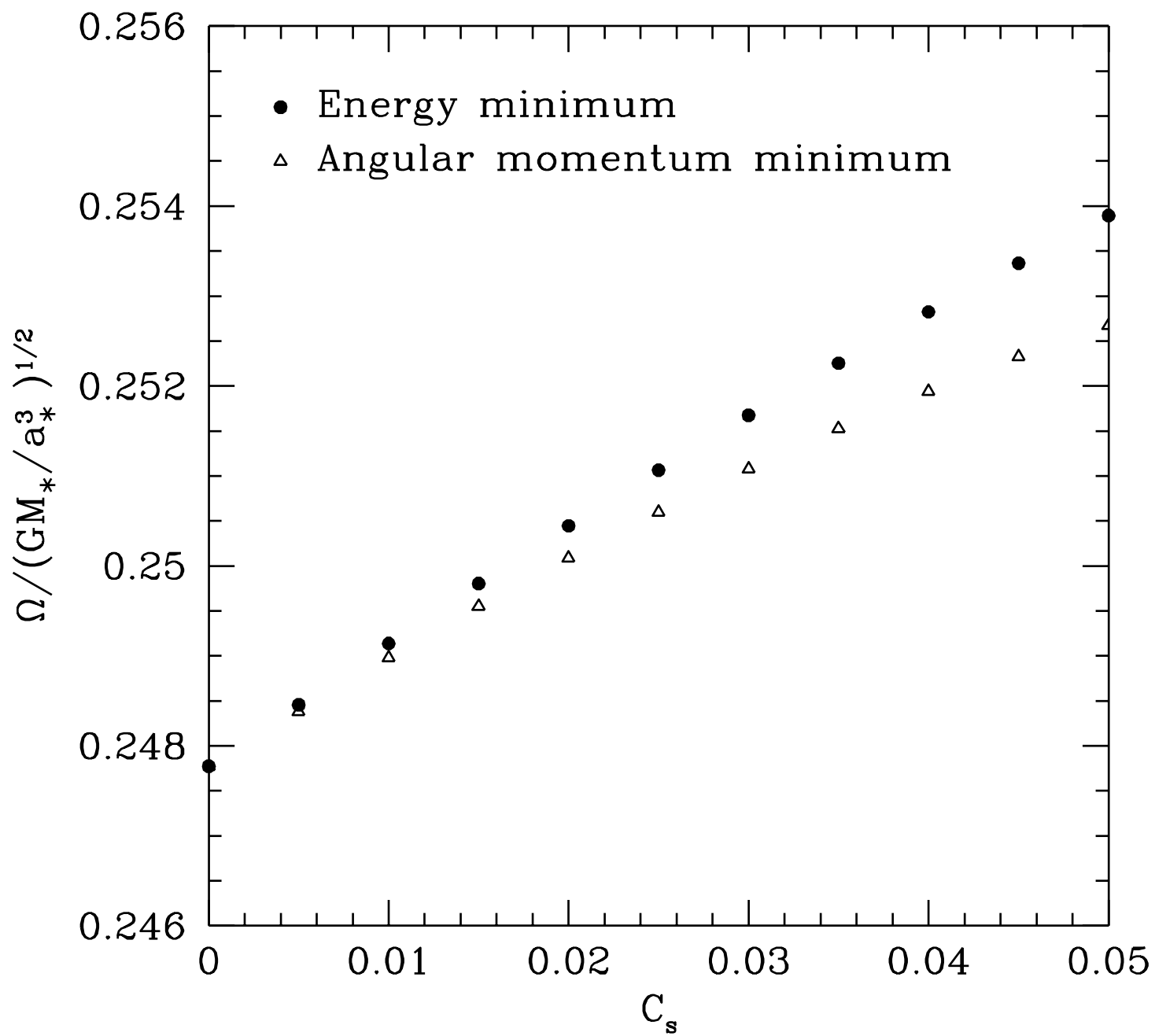


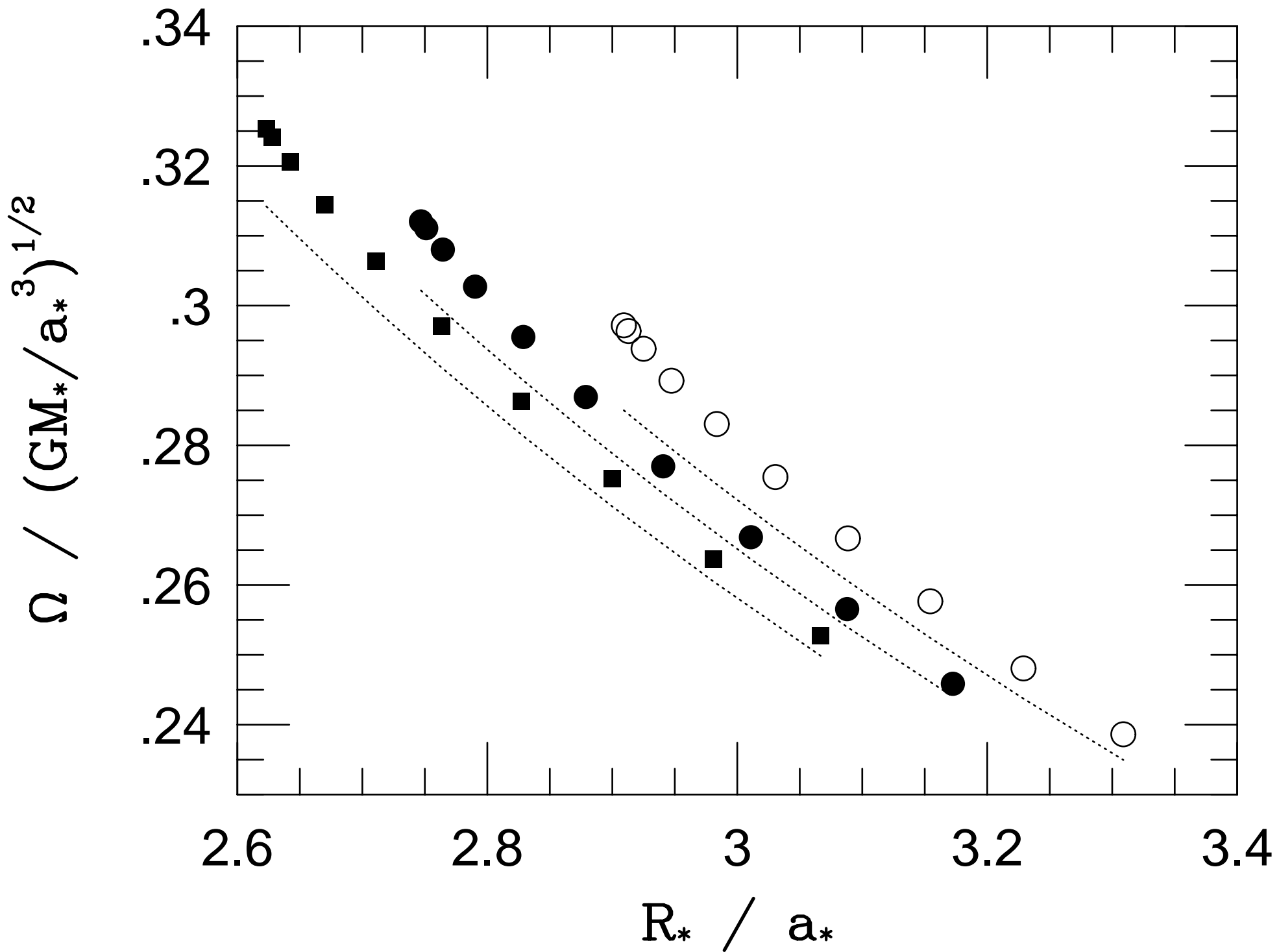


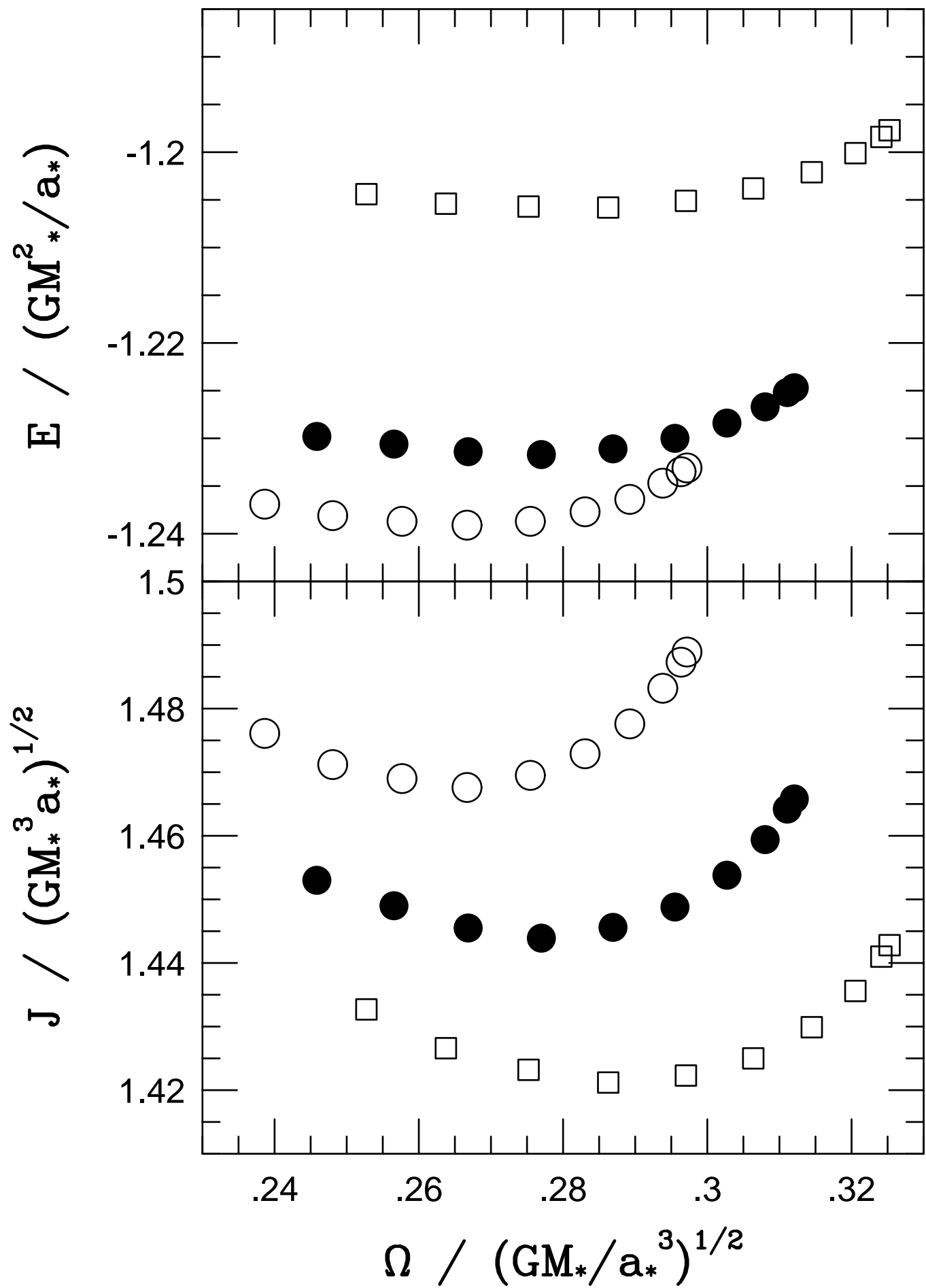
(a)

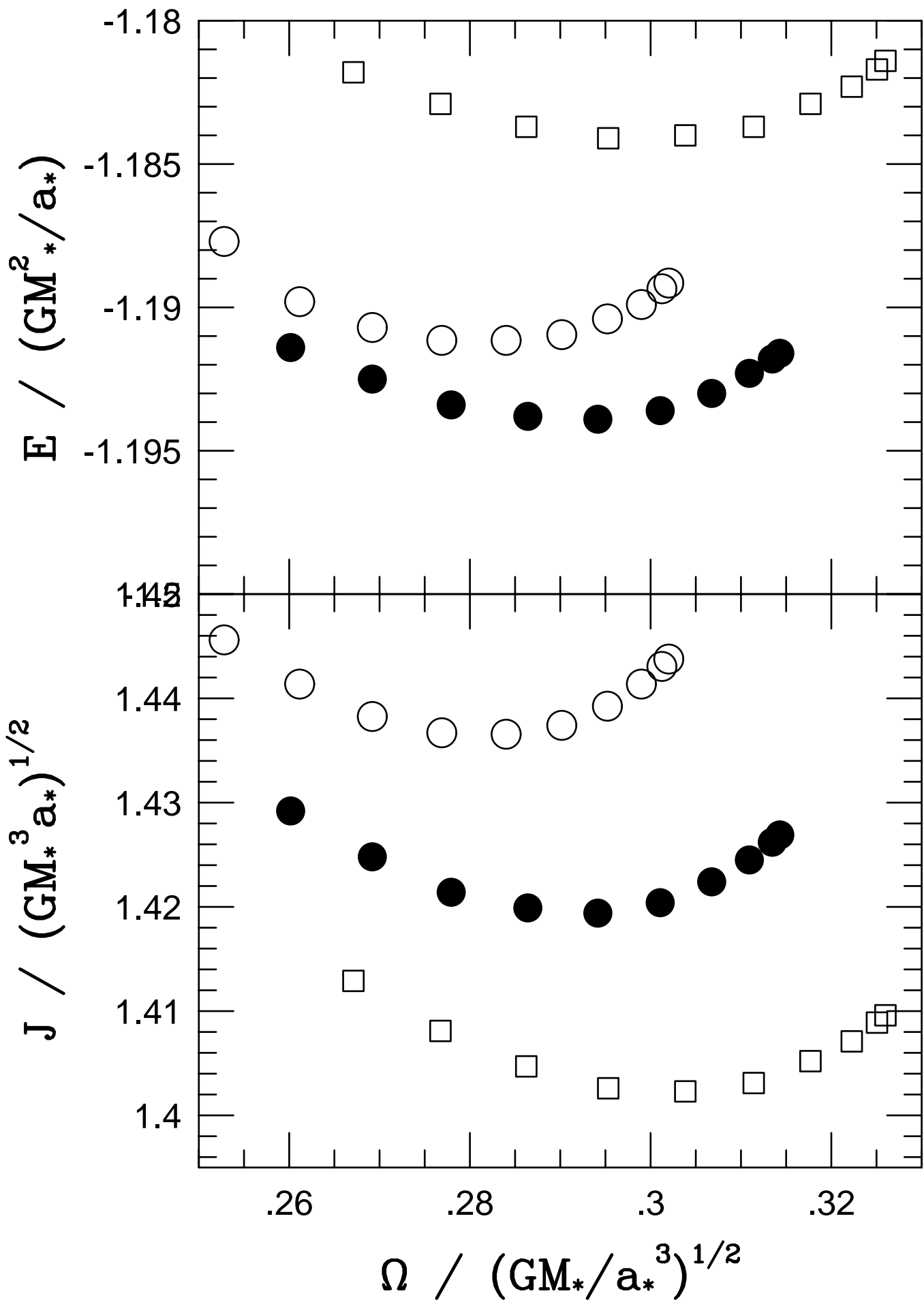


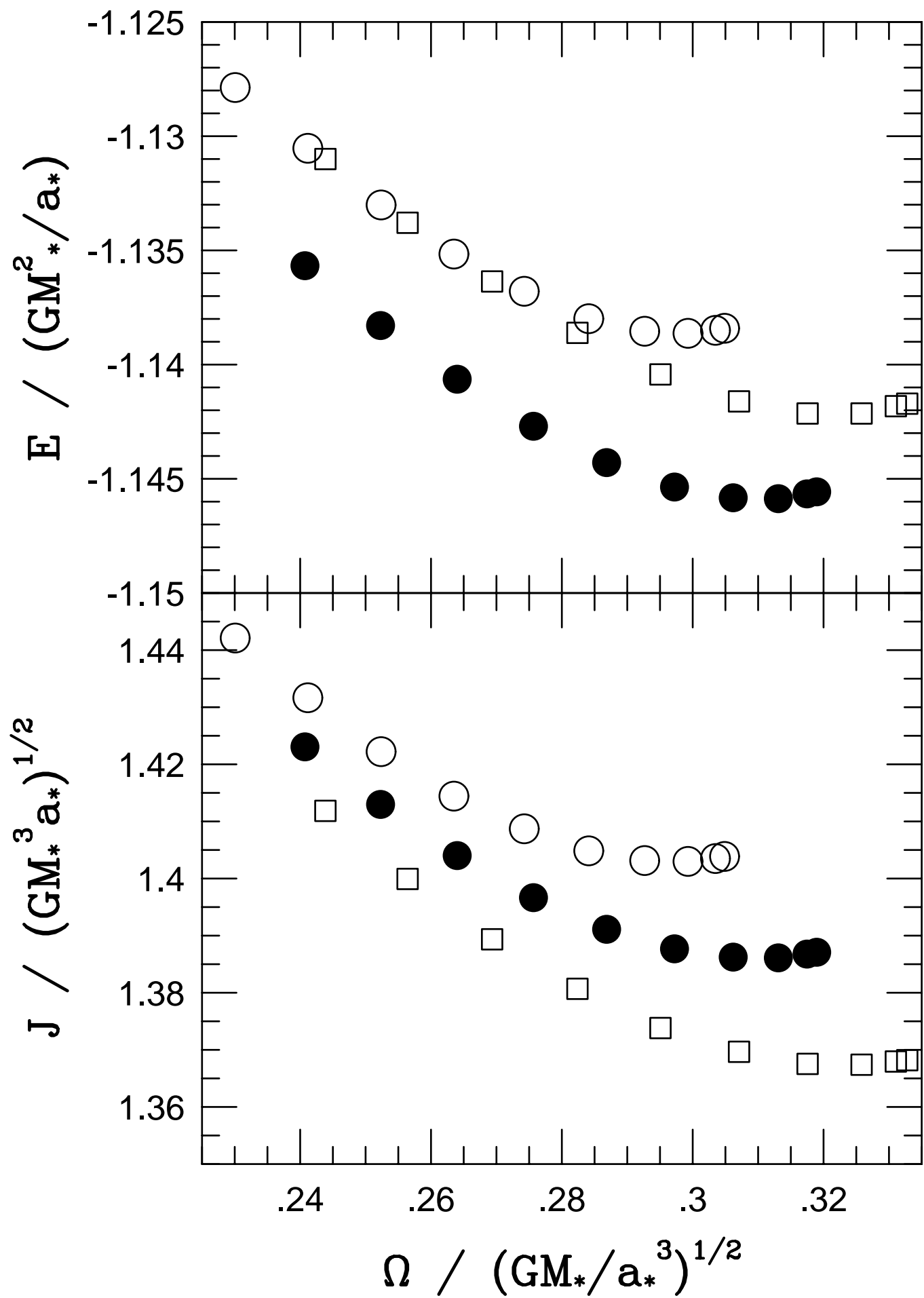
(b)

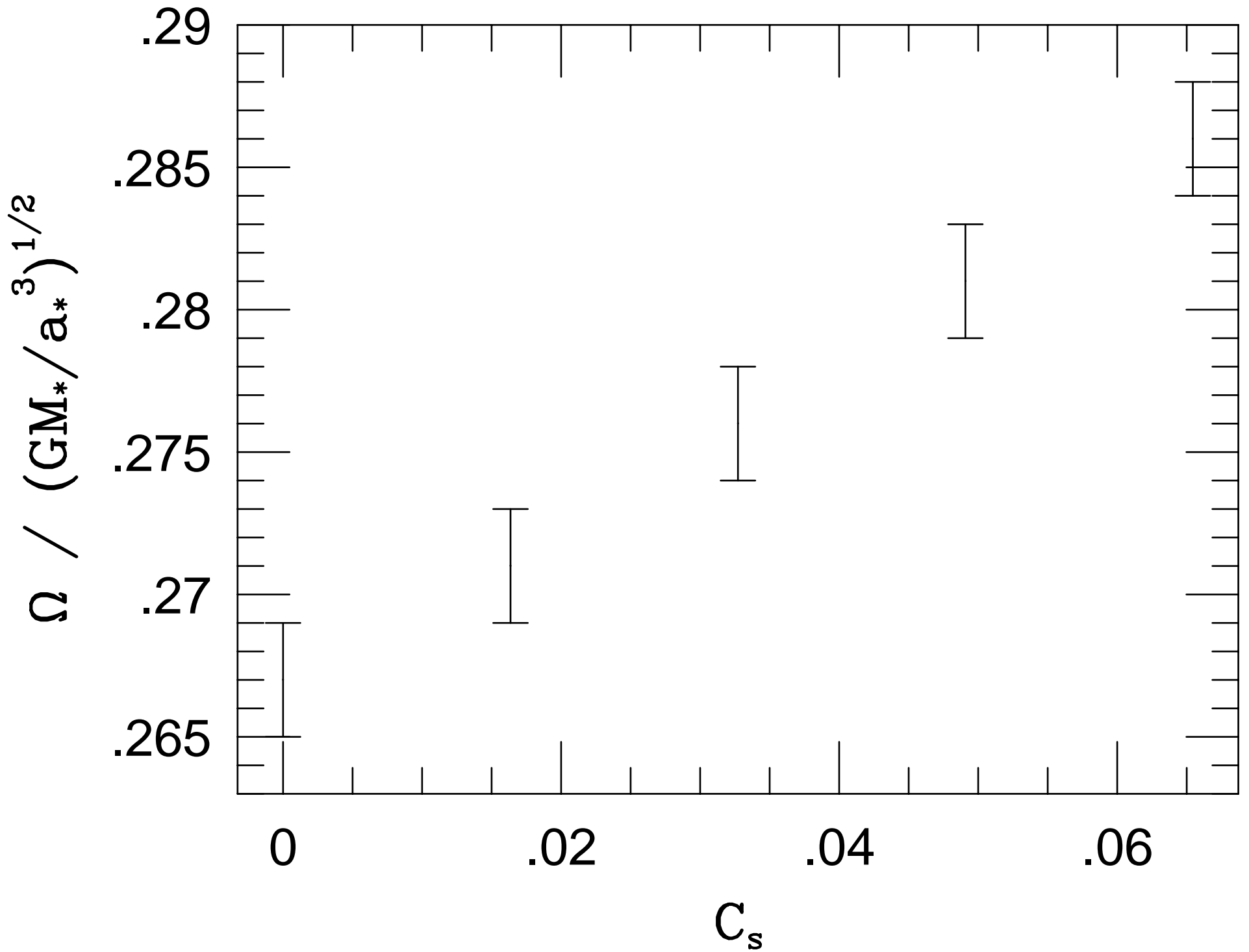


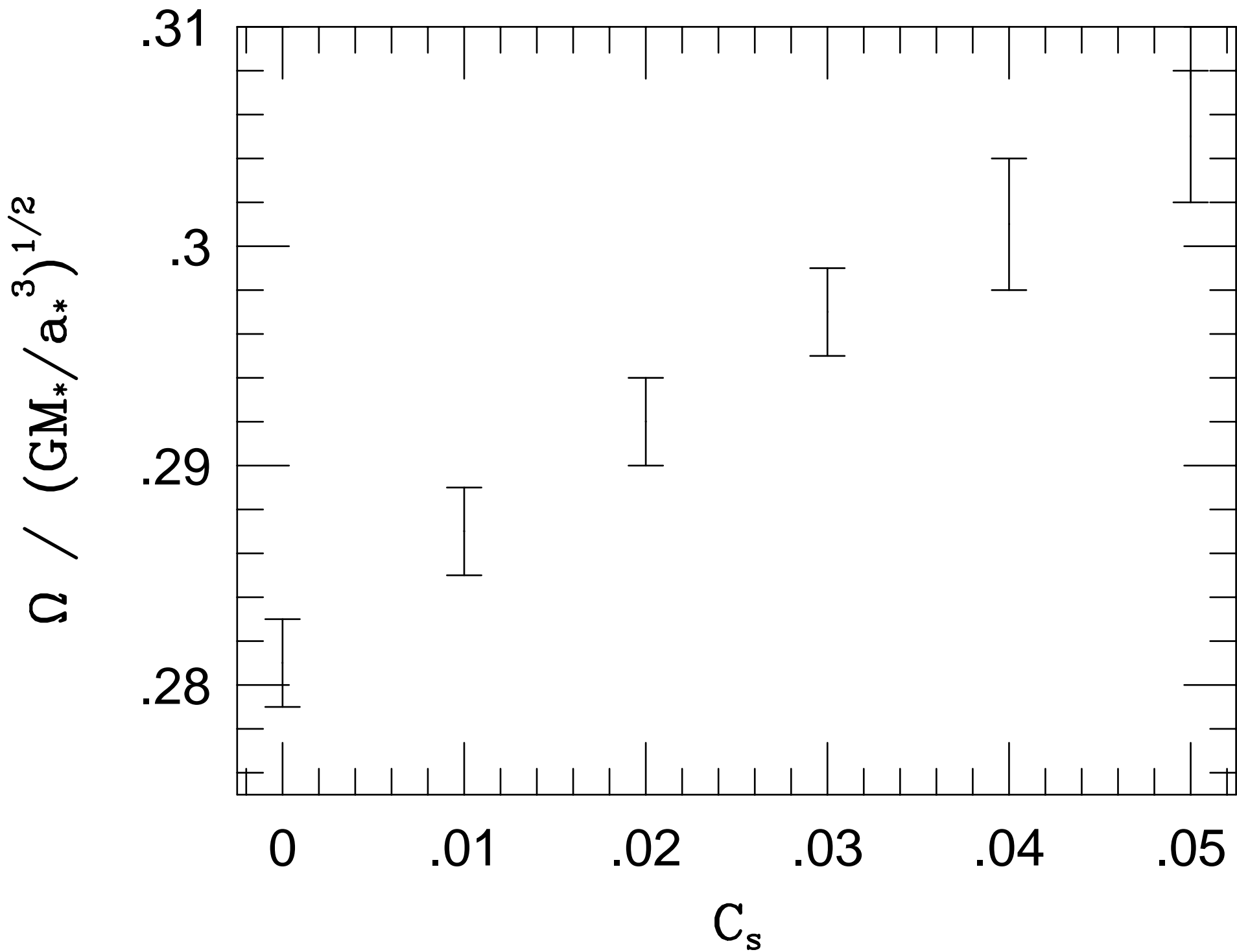


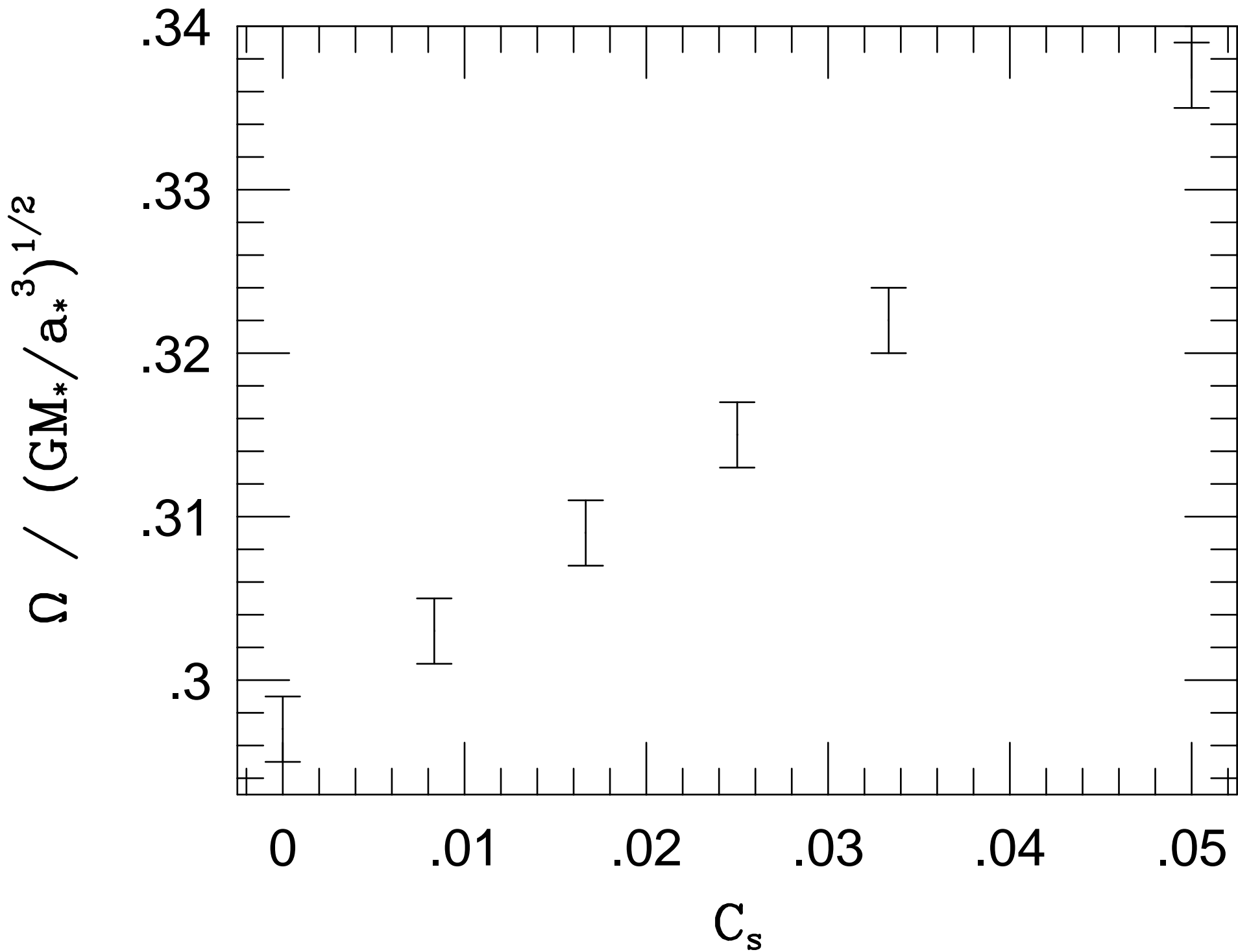


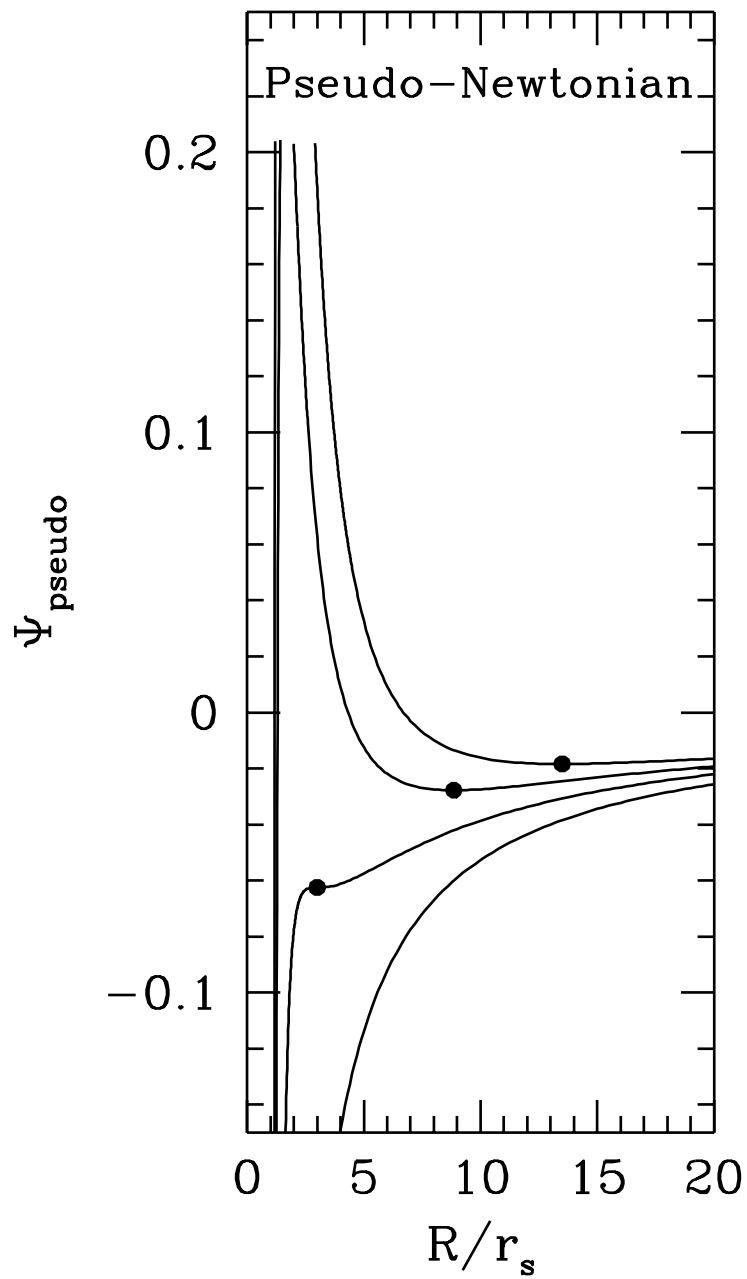
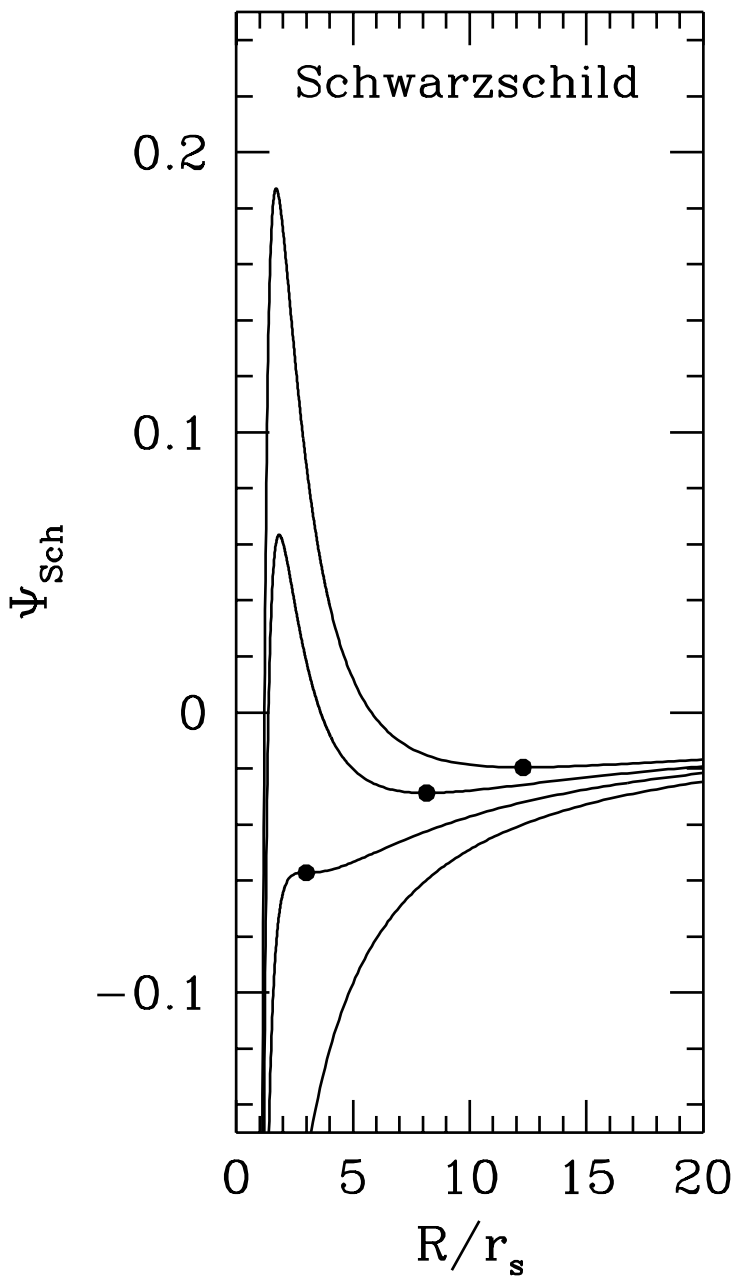




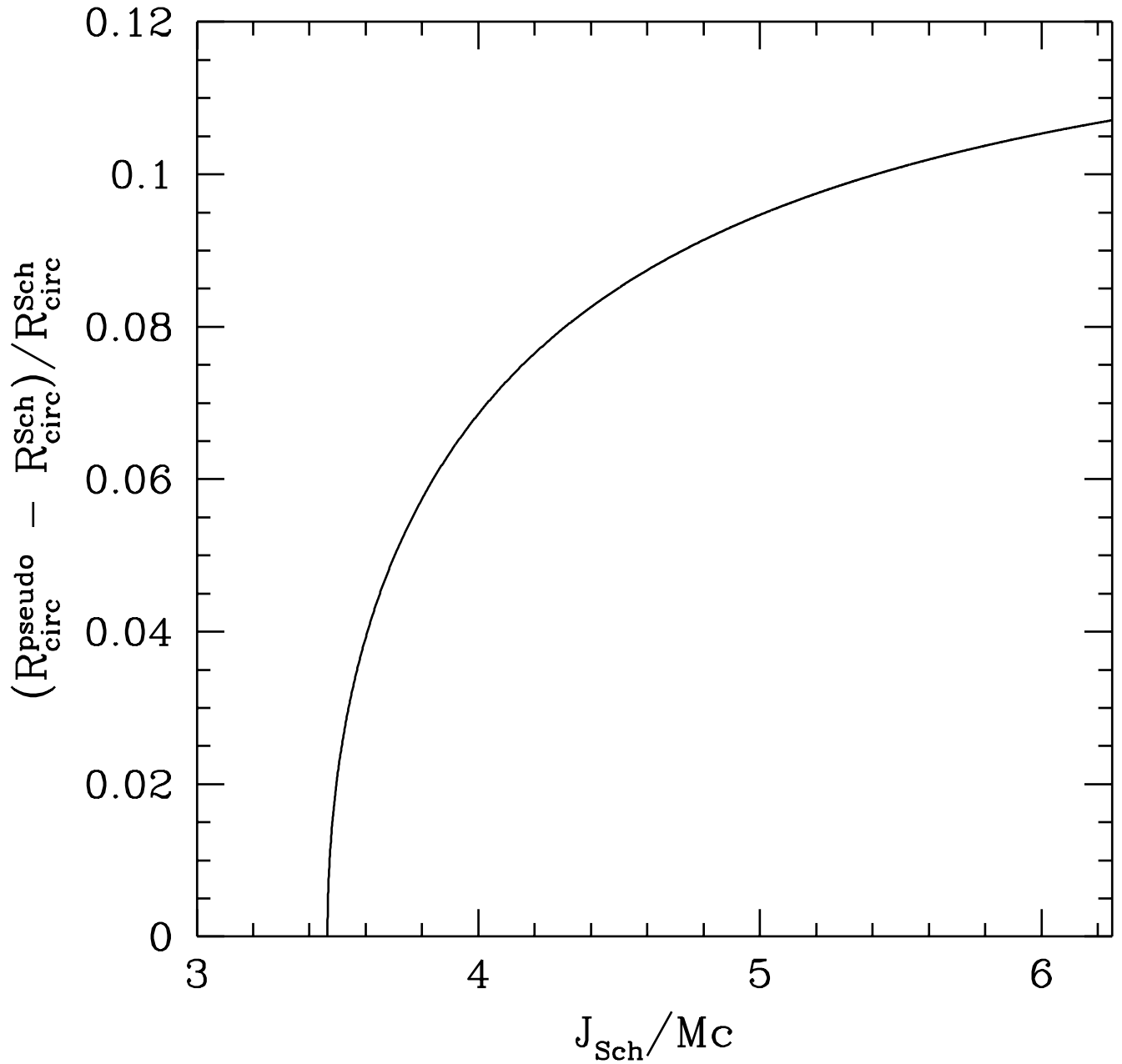




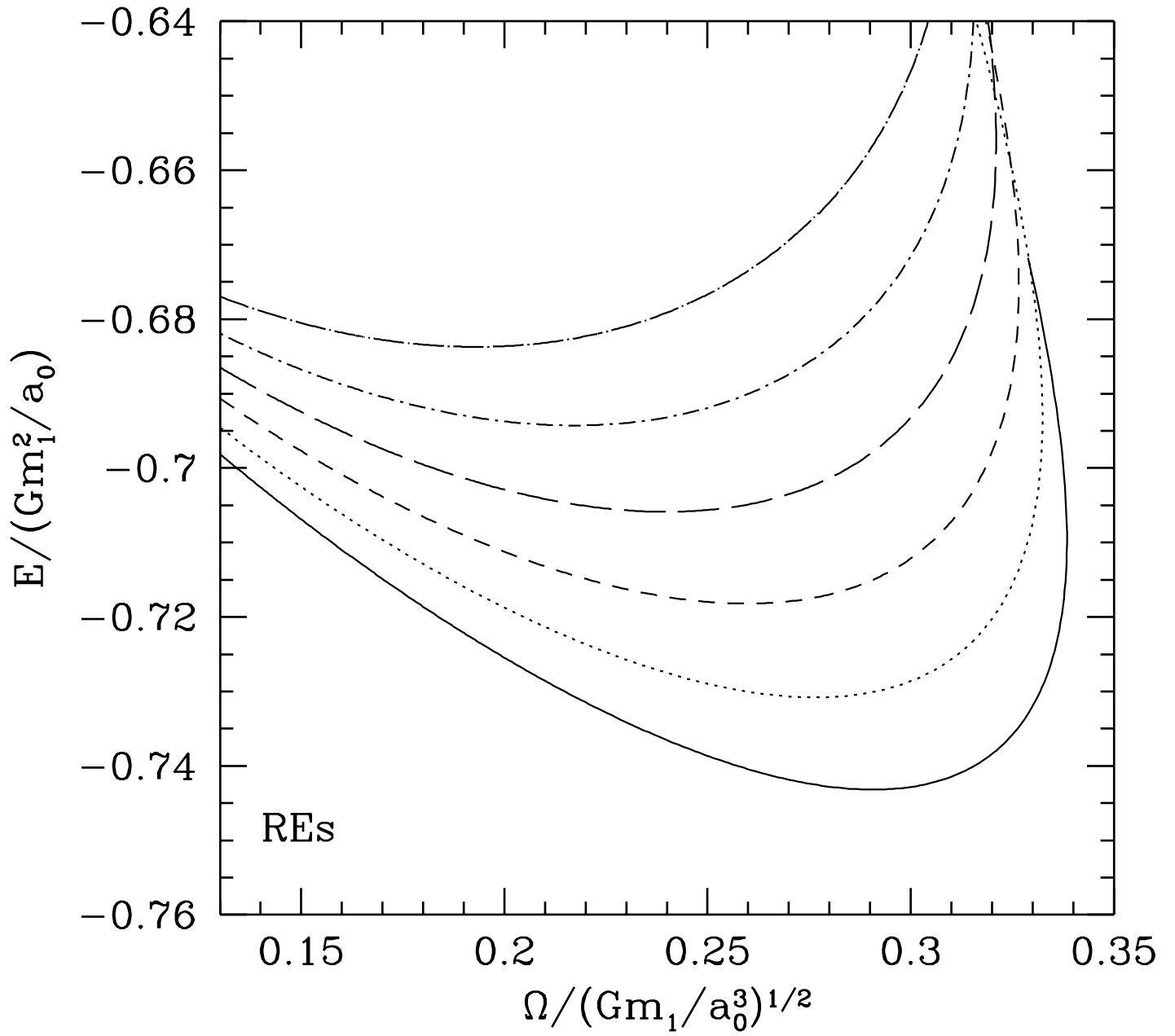




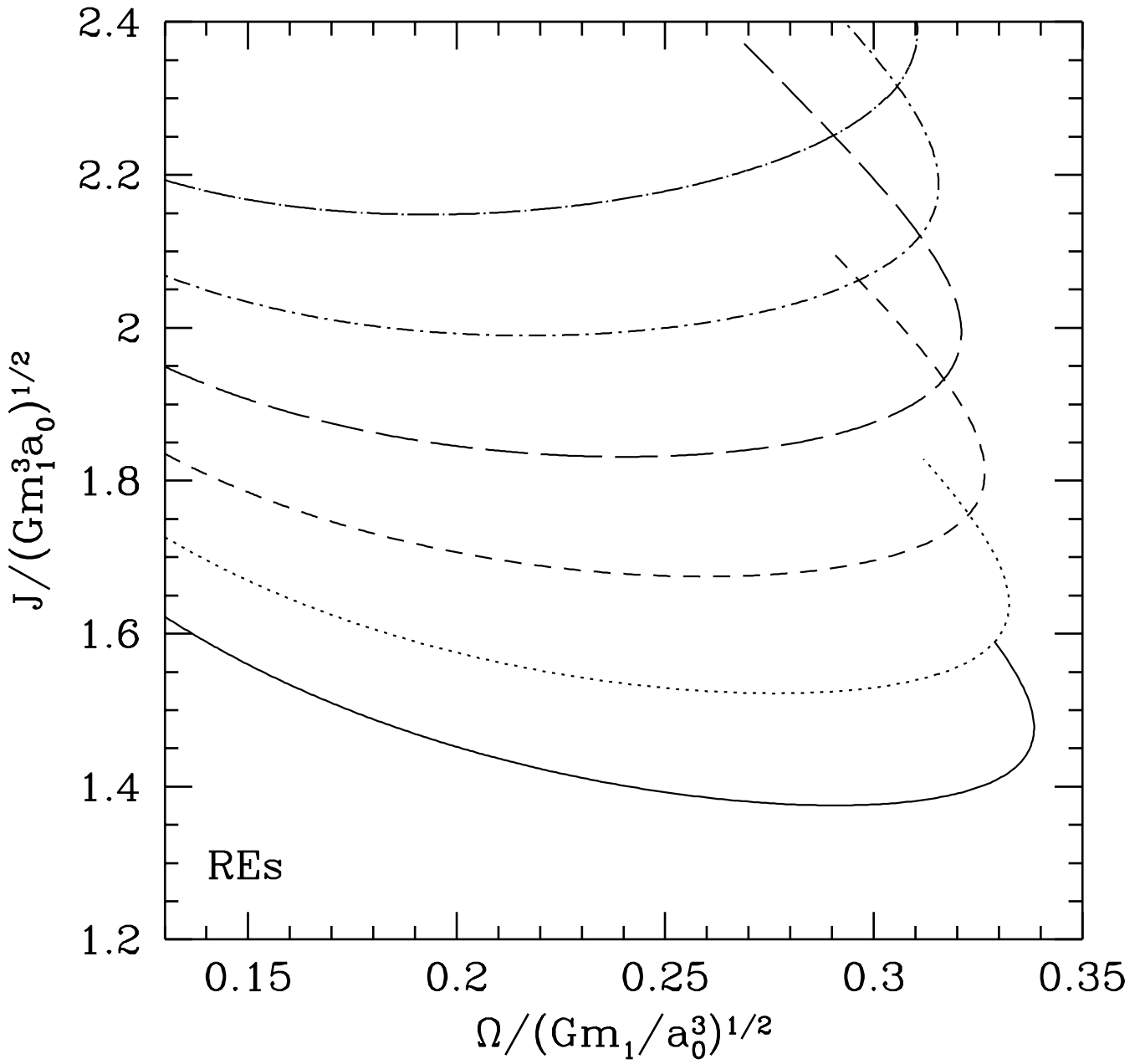
(a)



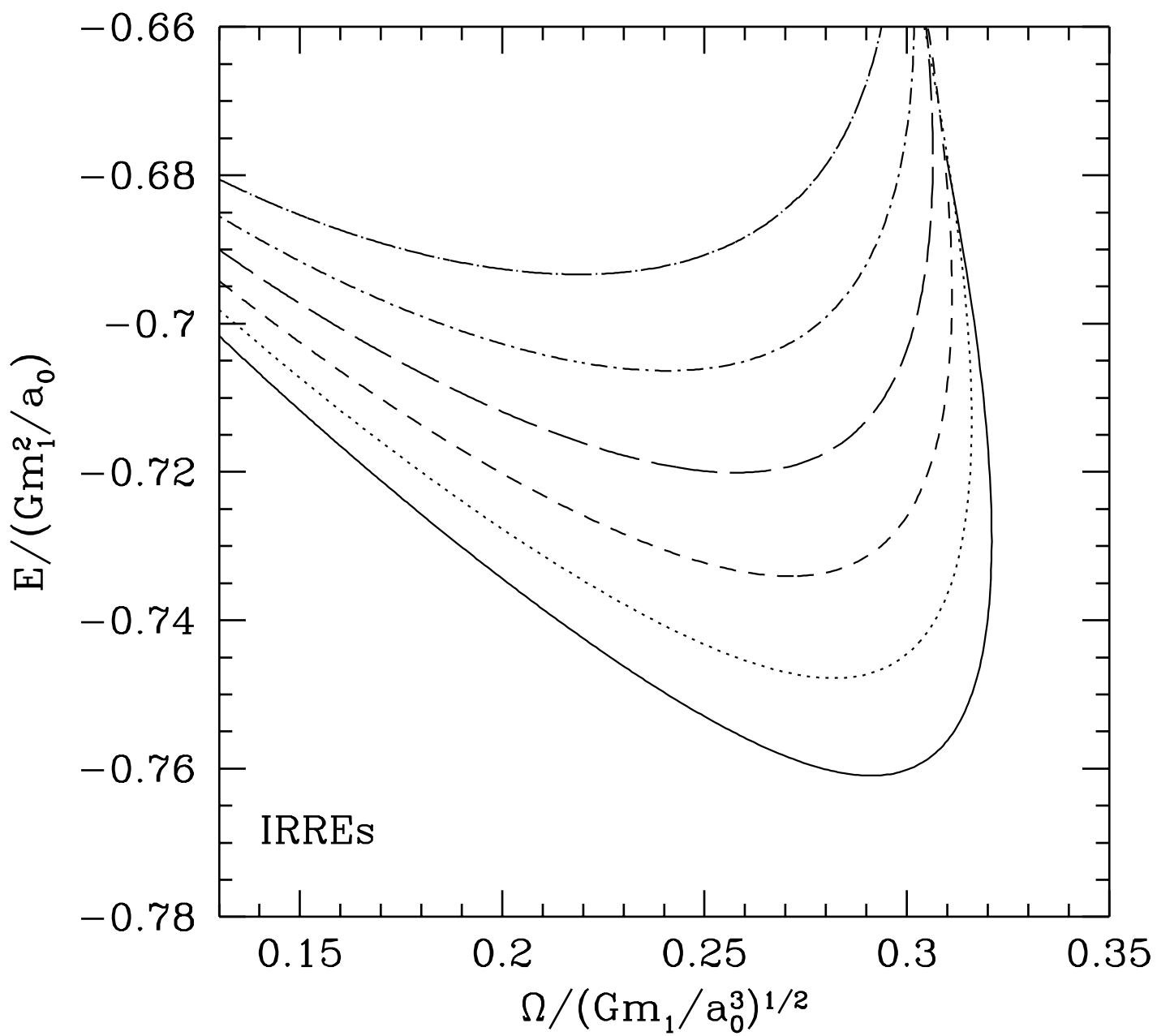
(b)



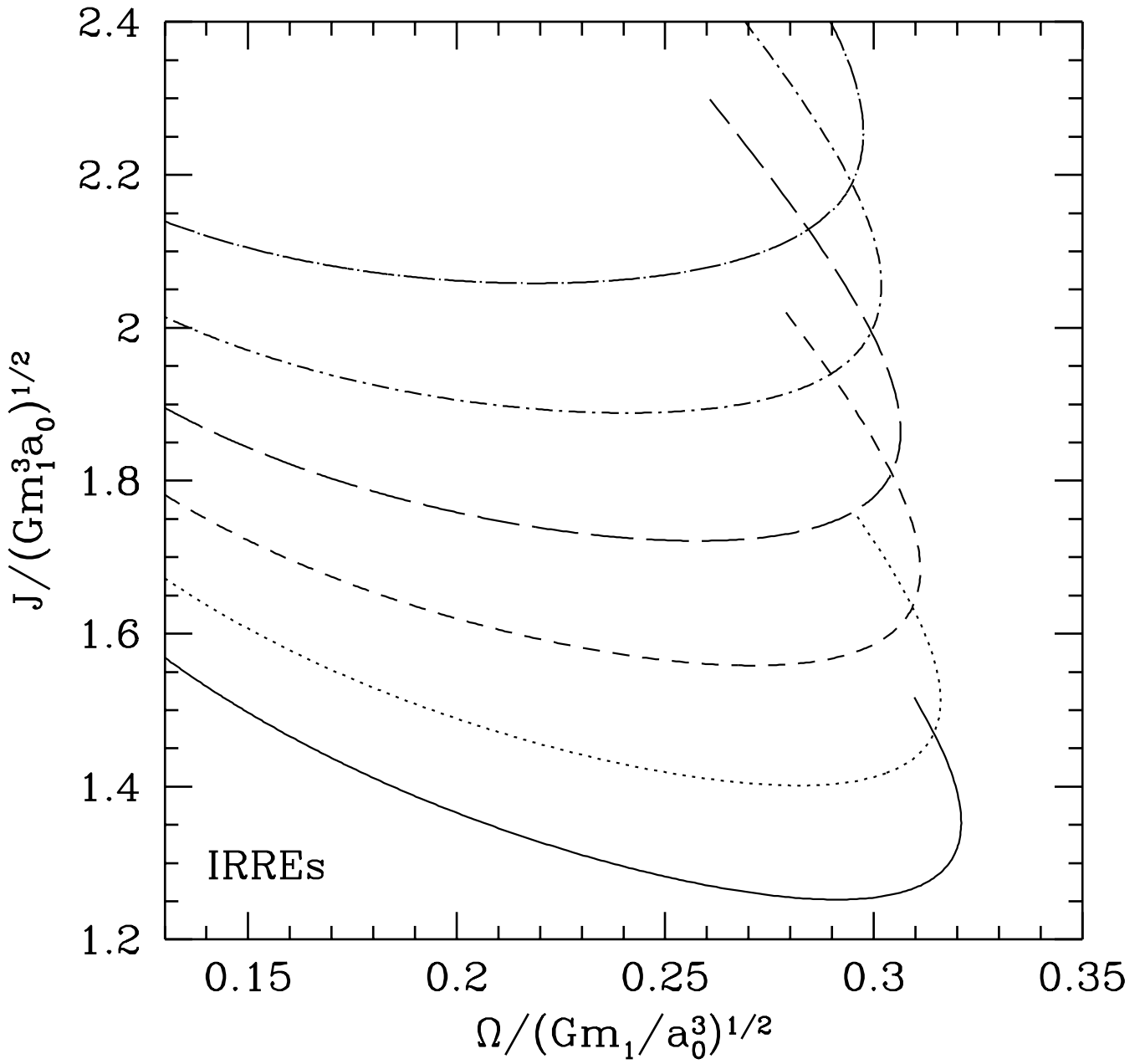
(a)



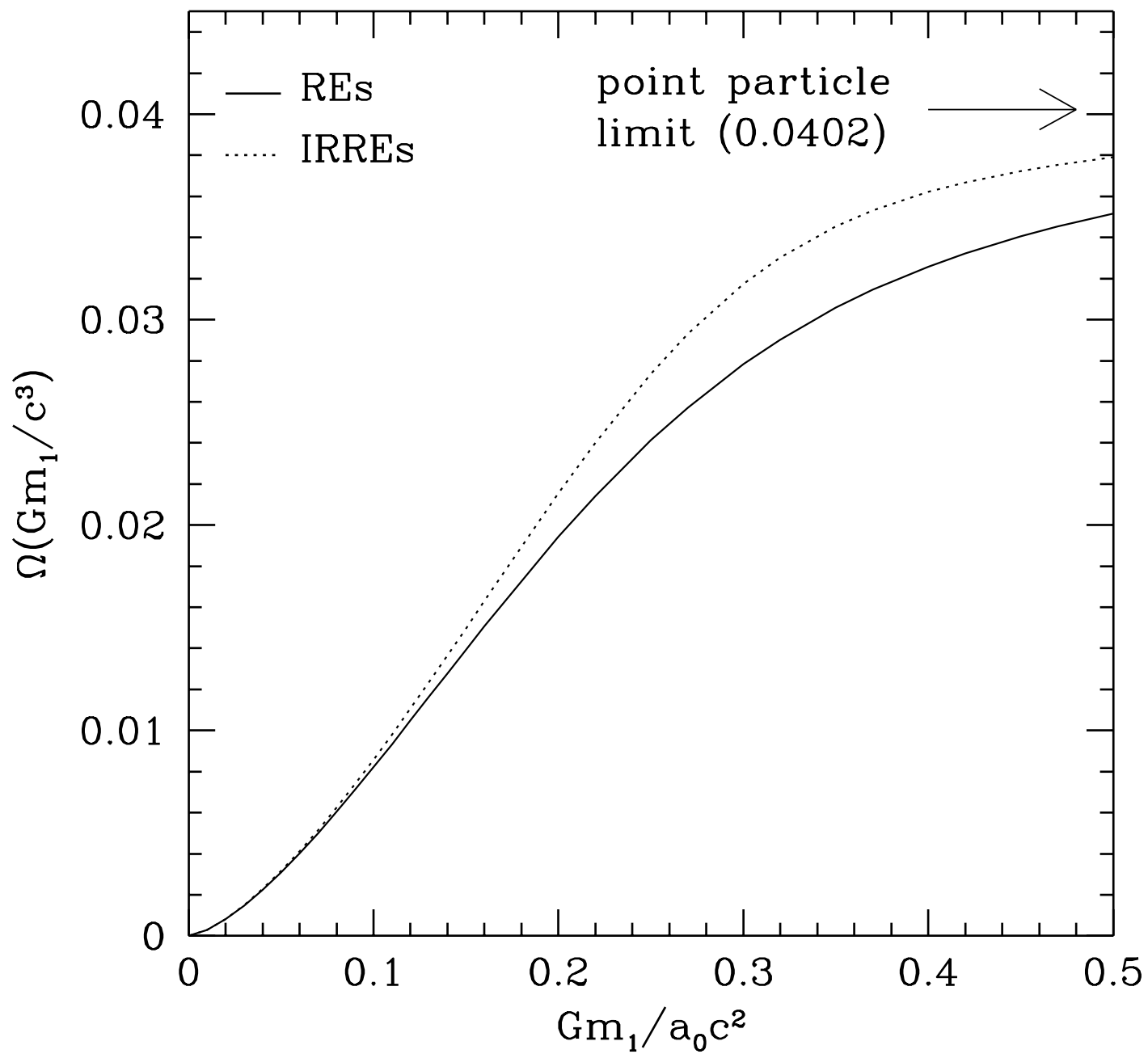
(b)

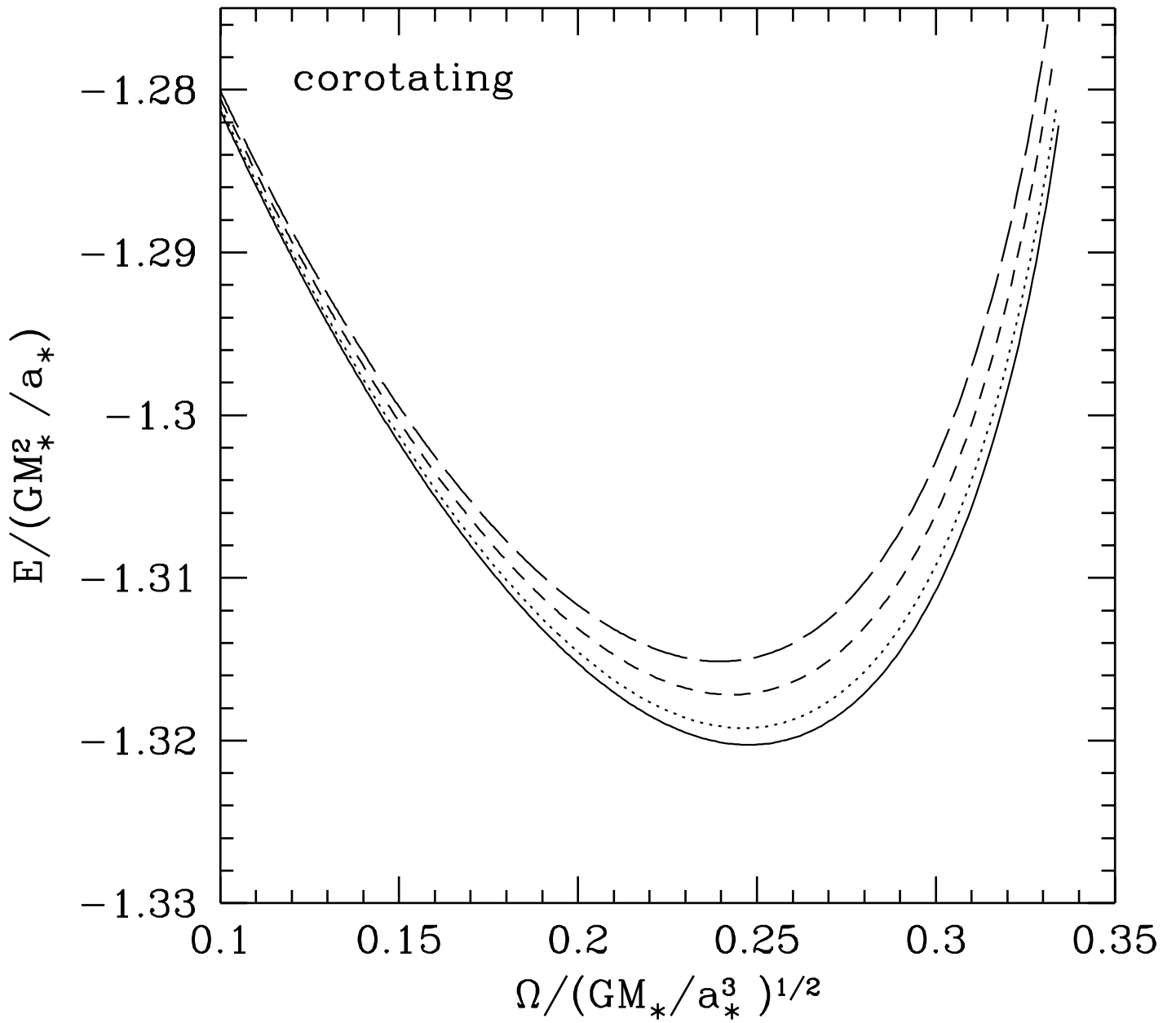


(a)

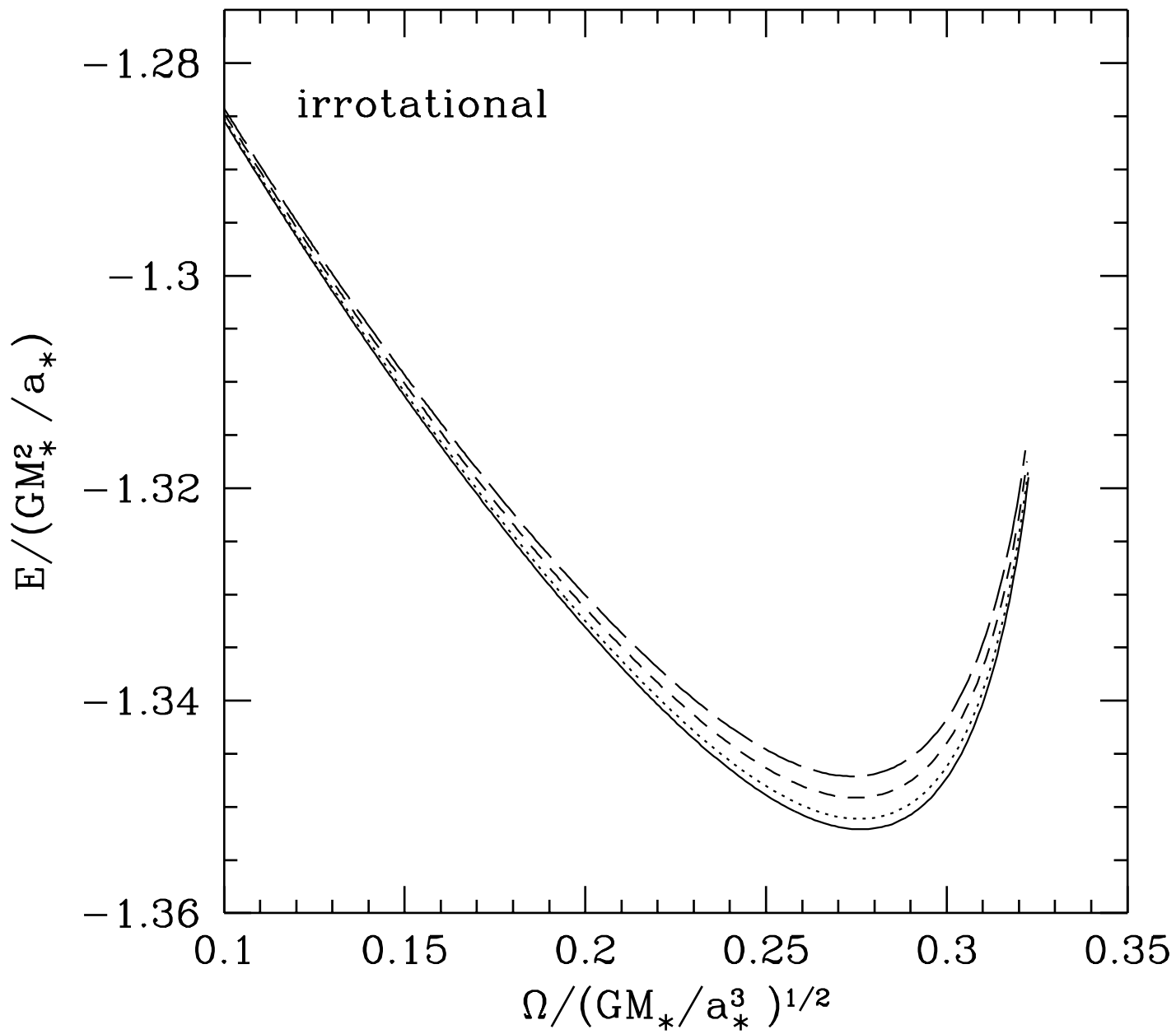


(b)





(a)



(b)

